

This is an Open Access document downloaded from ORCA, Cardiff University's institutional repository: <https://orca.cardiff.ac.uk/id/eprint/146852/>

This is the author's version of a work that was submitted to / accepted for publication.

Citation for final published version:

Shao, Longyi, Liu, Pengju, Jones, Tim , Yang, Shushen, Wang, Wenhua, Zhang, Daizhou, Li, Yaowei, Yang, Cheng-Xue, Xing, Jiaoping, Hou, Cong, Zhang, Mengyuan, Feng, Xiaolei, Li, Wenjun and Bérubé, Kelly 2022. A review of atmospheric individual particle analyses: methodologies and applications in environmental research. *Gondwana Research* 110 , pp. 347-369. 10.1016/j.gr.2022.01.007

Publishers page: <http://dx.doi.org/10.1016/j.gr.2022.01.007>

Please note:

Changes made as a result of publishing processes such as copy-editing, formatting and page numbers may not be reflected in this version. For the definitive version of this publication, please refer to the published source. You are advised to consult the publisher's version if you wish to cite this paper.

This version is being made available in accordance with publisher policies. See <http://orca.cf.ac.uk/policies.html> for usage policies. Copyright and moral rights for publications made available in ORCA are retained by the copyright holders.





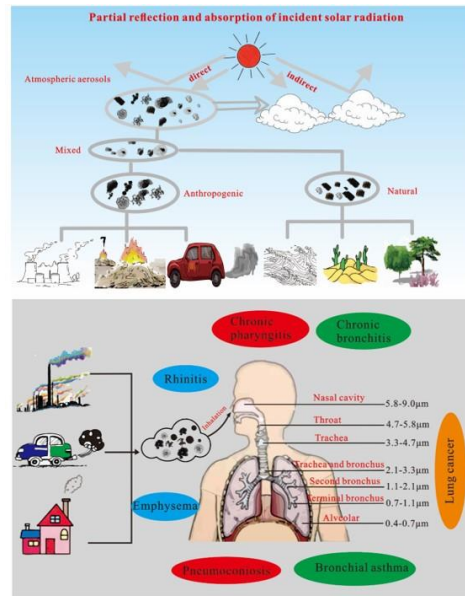
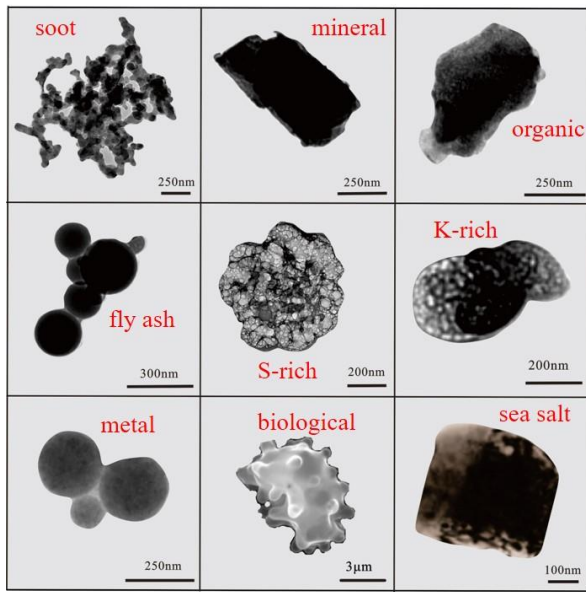
25        Highlights

26

- 27        1.    The techniques of individual particle analyses are summarized.
- 28        2.    The classification systems of the individual particles are reviewed.
- 29        3.    Possible sources of individual primary and secondary particles are discussed.
- 30        4.    Application of individual particle analysis in the environmental research are
- 31        introduced.

32

33 Graphical Abstract



34

35

36 **Abstract**

37 Aerosol ultra-fine and nano-particles are playing essential roles in the evolution of  
38 the Earth environment because of their deep connections to the chemical conversions  
39 and solar radiation energy transfer in the atmosphere, and have also become an urgent  
40 public concern in recent years due to their adverse health effects. Electron microscopes,  
41 as major tools being able to accurately identify the physical and chemical characteristics  
42 of individual particles in micron and submicron size, have been widely used in aerosol  
43 studies, although some barriers remain for their low efficiency and high cost. In this  
44 work, current understandings on the physical and chemical characteristics, mixing state  
45 and heterogeneous chemical reactions of individual aerosol particles, mainly obtained  
46 with electron microscopes, are reviewed. First, the techniques of individual particle  
47 analyses are briefly summarized and their advantages and disadvantages are discussed.  
48 Then, the morphology and composition of major atmospheric particle types obtained  
49 with these techniques and how the information was used to identify particle sources are  
50 introduced. The effects of aerosol particles on the environment, climate, human health,  
51 and global geochemical cycles are also discussed based on the data from individual  
52 particle analyses. Finally, challenges faced in individual particle studies are prospected.

53 **Keywords:** climate, electron microscope, global geochemical cycles, health,  
54 individual particle analyses, particle source

55

## 56 **1 Introduction**

57 Airborne particulate matter is a general term for all types of solid and liquid  
58 particles in the atmosphere (Tang et al., 2006), which is an atmospheric pollutant that  
59 is potentially harmful to human health (Dockery et al., 1993). Aerosol in atmospheric  
60 science generally refers to the suspension system of solid particles, liquid particles, or  
61 both of them in a gaseous medium (Freney et al., 2010). PM<sub>10</sub> refers to particulate  
62 matter in the ambient air that has an aerodynamic equivalent diameter of less than or  
63 equal to 10µm; also known as inhalable particulate matter. PM<sub>2.5</sub> refers to particulate  
64 matter in the ambient air that has an aerodynamic equivalent diameter of less than or  
65 equal to 2.5µm; also usually known as fine particulate matter (Jones et al., 2021).  
66 Ultrafine particle refers to particulate matter in the ambient air with an aerodynamic  
67 equivalent diameter of less than or equal to 0.1µm, also known as nanoparticles (Shao  
68 et al., 2000; Cao et al., 2014; Manigrasso et al., 2020; Naing and Lee, 2020).  
69 Atmospheric particulate matter is from natural and anthropogenic sources. Natural  
70 sources typically include emissions from crustal dust, wildfires, volcanic eruptions or  
71 resuspended volcanic ash, biological emission such as pollen and spores, and sea spray,  
72 in addition to particles produced via gas-to-particle conversions in the atmosphere (Li  
73 et al., 2016b; Oliveira et al., 2021; Trejos et al., 2021). The main anthropogenic sources  
74 include fuel combustion, industrial process, waste incineration and agricultural activity  
75 emissions (Silva et al., 2021). Atmospheric particulate matter released from  
76 anthropogenic sources is an important air pollutant ( Chan and Yao, 2008; Bi et al.,  
77 2011). For example, industrial processes can emit large numbers of fugitive dust  
78 particles (Cheng et al., 2020); incineration of solid waste can release large numbers of  
79 soot particles (He et al., 2021); agricultural activities can emit large quantities of  
80 potassium-rich (K-rich) particles (Bi et al., 2011; Singh et al., 2018). The continuous  
81 accumulation of particles in the atmosphere and the increase of particle concentrations  
82 facilitate the formation of haze under certain meteorological conditions (Shen et al.,  
83 2021). Frequent haze events pose a significant threat to human health, even leading to  
84 increased numbers of mortality (Oberdorster et al., 1995; Pope et al., 1995; Garcia-

85 Hernandez et al., 2019). When particles are inhaled, they can cause a variety of health  
86 hazards including asthma, lung function decline and respiratory inflammation, and can  
87 also affect the cardiovascular, nervous, and immune systems (Daigle et al., 2003;  
88 Oberdorster et al., 2004; Pope and Dockery, 2006; Chai et al., 2019;). In addition,  
89 atmospheric particles can also directly or indirectly affect the climate. Sulfate particles  
90 reflect incident solar radiation (Krishnamohan et al., 2020); carbonaceous particles can  
91 absorb sunlight, leading to positive radiative forcing and global warming (McMeeking  
92 et al., 2011). Sea salt particles play a dual role in atmospheric radiation balance,  
93 scattering incoming solar radiation and absorbing ground radiation, thus directly  
94 affecting climate (Ayash et al., 2008; Meesang et al., 2013). At the same time, sea salt  
95 particles can also act as cloud condensation nuclei, indirectly affecting climate (Ayash  
96 et al., 2008). The absorption by brown carbon was noted to be highest in winter,  
97 accounting for 41% of the total absorption (Zhu et al., 2021). Another study found that  
98 sulfates and organic matter acted as coating materials enclosing the soot particles (Yuan  
99 et al., 2019), enhancing the light absorption capacity compared to the uncoated soot  
100 particles (Wang et al., 2017).

101 There are diverse research methods that can be applied to atmospheric particles.  
102 These methods are divided into bulk sample analysis and individual particle analysis.  
103 Bulk sample analysis has involved a variety of instrumental tests. Inductively Coupled  
104 Plasma Mass Spectrometer (ICP-MS) is a common method for bulk sample chemical  
105 composition analysis, which can be used to measure metal levels (Ari et al., 2020).  
106 Inductively Coupled Plasma-Optical Emission Spectroscopy (ICP-OES) is used to  
107 measure inorganic elements (Zalakeviciute et al., 2020). Ion Chromatograph (IC) is  
108 used to measure water-soluble ions (Rodriguez et al., 2020). Inductively Coupled  
109 Plasma Atomic Emission Spectrometry (ICP-AES) is used for the determination of  
110 elements in a great variety of different types of samples (Menzel et al., 2002).  
111 Additionally, bulk sample measurement methods include Aerosol Mass  
112 Spectrometry (AMS) (Reyes-Villegas et al., 2018), Elemental-Carbon tester,  
113 Meteorological Gas Chromatograph Mass Spectrometry (GC-MS) (Choi et al., 2020),

114 High Performance Liquid Chromatography Mass Spectrometry (HPLC/MS) (Buiarelli  
115 et al., 2018), and Proton Transfer Reaction Mass Spectrometry (PTR-MS) (Maji et al.,  
116 2020).

117 In bulk sample analysis, various instruments can simultaneously analyze hundreds  
118 or thousands of aerosol particles and characterize the mass concentrations of different  
119 components in the particles. These batch methods can quantify different aerosol species,  
120 depending on the instrument (Li et al., 2016b). However, bulk sample analysis has  
121 many limitations, they cannot provide mixing state and surface properties of airborne  
122 particles. The mixing state of particles is of great significance in the study of regional  
123 haze (Li et al., 2016b; Saikia et al., 2018). Due to the limitation of bulk sample analysis,  
124 individual particle analysis technology has been developed, which makes up for the  
125 deficiency of bulk sample analysis well.

126 Individual particle analysis was first used to analyze aerosol particles with an  
127 electron microscope in 1967 (Frank and Lodge, 1967). Bigg et al. (1974) developed  
128 vapour-deposited thin film method to test sulfate particle under electron microscope.  
129 Ayers et al. (1977) improved this method in 1977. With the development of  
130 measurement technology, microanalysis technology has been applied to the study of  
131 individual aerosol particle in the atmosphere. Ramsden and Shibaoka, (1982) studied  
132 the morphology and chemical composition of soot particles by scanning electron  
133 microscopy, transmission electron microscopy and EPMA (Electron Probe X-ray  
134 Micro-Analysis). Iwasaka et al. (1988) observed the morphology of individual particles  
135 in the height range from near the ground to about 4400m with electron microscope and  
136 found that particles were very frequently transported from Asian desert areas to the  
137 islands of Japan in the middle troposphere. In 1990s, many references on individual  
138 particle analysis have emerged. Individual particle analysis techniques began to be  
139 applied to mineralogy, morphology, chemical composition, and the relationship  
140 between various effects of particulate matter. Liu et al. (1994) analyzed atmospheric  
141 particulate matter in Qingdao and found that the sources of particulate matter mainly  
142 included soil dust, coal burning, cement industry, fuel oil and steel industry. Prospero



143 et al. (1999) studied the long-distance transport of sand dust in the southeastern United  
144 States affected by African dust storms and concluded that kaolinite is mainly located in  
145 low latitudes in West Africa, while illite is mainly located in northern regions to the  
146 Mediterranean coast. Zhang et al. (1998) made a preliminary classification of the  
147 morphology of particles, and analyzed individual sulfate particles and sand particles  
148 with EDX respectively. In the early stage of individual particle analysis, many other  
149 researchers have made outstanding achievements (Mamane and Noll, 1985; De Bock  
150 et al., 1994; Yamato and Tanaka, 1994; Katrinak et al., 1995;).

151 In recent years, individual particle analysis became an indispensable methodology.  
152 The development of high-resolution micro-electronics has improved the use of this  
153 method, with particulate matter identification more accurate. In this review, we  
154 summarize the individual particle analysis techniques, including Scanning Electron  
155 Microscopy (SEM) coupled with Energy Dispersive X-ray spectrometry (EDX),  
156 Transmission Electron Microscopy (TEM) coupled with Energy Dispersive X-ray  
157 spectrometry (EDX), Surface-Enhanced Raman Scattering (SERS), Spectroscopy  
158 Scanning Transmission X-ray Microscopy (STXM), Scanning Transmission X-ray  
159 Microscopy with Near-edge X-ray Absorption Fine-structure (STXM-NEXAFS),  
160 Atomic Force Microscopy (AFM), Nanometer-scale Secondary Ion Mass Spectrometry  
161 (Nano-SIMS), Time of Flight Secondary Ion Mass Spectrometry (TOF-SIMS), Single  
162 Particle Aerosol Mass Spectrometry (SPAMS), Aerosol-Time-Of-Flight Mass  
163 Spectrometry (ATOFMS), Ultrafine Aerosol Time-Of-Flight Mass Spectrometer (UF-  
164 ATOFMS), and Micro-Raman Spectroscopy (Micro-RS) without SERS. Most of  
165 individual particle analysis techniques use high-energy particle beam incident on  
166 particle surface and collect physical signals excited by the interaction between high-  
167 energy particle beam and particle surface atoms to obtain information about individual  
168 particle. These individual particle analysis techniques can provide detailed insights into  
169 particle origin, formation, migration, reactions, mixing mechanisms, aging status, and  
170 environmental effects, and human health impact.

171 In this review, the technologies used to analyze individual particles, the type of

172 individual particles appropriate for these techniques, the sources of individual particles  
173 and their characteristics, and the influence and behavior of individual particles  
174 (hygroscopicity, optical effects, climatic effects, transport, and health effects) are  
175 reviewed.

## 176 **2 Methodologies of individual particles analysis**

177 There are offline and online techniques in individual particle analyses. Offline  
178 methods for the individual particle analysis include SEM-EDX, TEM-EDX, SERS,  
179 STXM-NEXAFS, AFM, Nano-SIMS, and TOF-SIMS. Online methods and equipment  
180 for individual particle analysis include SPAMS, ATOFMS, UF-ATOFMS and Micro-  
181 RS.

182 SEM-EDX has high resolution (20nm) and is suitable for particles larger than  
183 100nm. SEM-EDX can obtain the three-dimensional morphological characteristics of  
184 particles and the element composition on the surface of particles, but only the  
185 information on the surface of particles (Li and Shao, 2010).

186 TEM-EDX has higher resolution (0.1nm) and is suitable for particles smaller than  
187 2 $\mu$ m. TEM-EDX can obtain internal information about particles but operating the  
188 TEM-EDX is complex and expensive, and its detection of N is poor (Li et al., 2016b;  
189 Xing et al., 2020). Cryogenic TEM and Scanning TEM are also methods under the  
190 category of TEM. Cryogenic TEM has advantages in detecting the microstructure of  
191 volatile atmospheric particles, excluding the influence of volatile component loss on  
192 particle morphology and composition (Li et al., 2021). Scanning TEM mode is more  
193 convenient for particle analysis than manual processing, saving a large amount of work  
194 and time (Yuan et al., 2021).

195 SERS is a comprehensive technology for sample detection, that is a good  
196 supplement to traditional electron microscopy methods. SERS is very effective in  
197 monitoring the mass concentration of sulfate and nitrate. In addition, SERS can observe  
198 the evaporative behaviour of sulfate under vacuum conditions, but it cannot provide  
199 images and particle size information (Sun et al., 2019).

200 STXM can study specific bond types in aerosols, as can Nano-SIMS and TOF-  
201 SIMS. The resolution of STXM images is 35nm, and the resolution of the energy  
202 spectrum is 100nm. STXM is suitable for particles greater than 100nm and can  
203 characterize the morphology and functional groups of aerosol particles, but the spatial  
204 resolution of STXM is low (Fraund et al., 2019).

205 AFM can also obtain the three-dimensional morphology of particles, which is  
206 suitable for particles smaller than 2 $\mu$ m. AFM can study the surface texture, viscosity,  
207 deformation, and elasticity of particles (Shi et al., 2015; Zhang et al., 2020a), but it  
208 cannot provide information about the composition of those particles.

209 Nano-SIMS is suitable for particles larger than 50nm and is sometimes used to  
210 study the isotopic characteristics of individual particles, but more often it is used to  
211 characterize the mixing state of aerosols, especially the mixing characteristics of  
212 organic matter, sulfate, and nitrate (Ghosal et al., 2014; Li et al., 2016a). However,  
213 Nano-SIMS is not suitable for statistical analysis because it requires manual operation  
214 and statistics and is also very expensive.

215 TOF-SIMS is suitable for particles larger than 100nm and can obtain the surface  
216 chemical composition of aerosol particles, the depth distribution of chemical  
217 components, surface, and three-dimensional images (Tervahattu et al., 2002; Lazzeri et  
218 al., 2003), but the spatial resolution is low.

219 SPAMS uses a high-energy pulsed laser as the ionization source, which can  
220 analytically ionize almost all kinds of particles. SPAMS is used for particles larger than  
221 100nm, and the main particle size range is 0.2-2.5 $\mu$ m. SPAMS can obtain the chemical  
222 composition and size information of particles, but it cannot provide the images of those  
223 particles (Chen et al., 2017b; Peng et al., 2020; Shen et al., 2020).

224 ATOFMS/UF-ATOFMS uses aerodynamic lens focused injection and provides  
225 real-time size and chemical composition data of individual particles using a dual laser  
226 caliper system and a two-stage Time-Of-Flight Mass Analyzer (Toner et al., 2006).  
227 ATOFMS can detect a particle size range of 0.1 $\mu$ m-3 $\mu$ m (Gard et al., 1997). Different  
228 versions of ATOFMS can measure different compositions of aerosol particles, such as

229 organic matter, sulfate, nitrate, metal, and mineral (Middlebrook et al., 2003). UF-  
230 ATOFMS instrument incorporated an aerodynamic lens for improving transmission of  
231 smaller accumulation mode and ultrafine particles. UF-ATOFMS can provide a particle  
232 size range of 50-300nm (Toner et al., 2008), but cannot provide individual particle  
233 images.

234 Micro-RS collects spectral data corresponding to molecules and functional groups  
235 under normal ambient conditions and can monitor the changes in morphology and  
236 chemical composition of individual particles during their reaction with trace gases.  
237 Micro-RS without SERS was also used to detect the chemical composition of individual  
238 atmospheric particles (Wang et al., 2021b).

239 In general, although online individual particle analysis is more convenient and has  
240 a higher efficiency in the chemical characterization of pollutants, what is obtained is  
241 still the overall chemical compositions of the particulate matters, and the method cannot  
242 provide detailed information on the internal structure and the inhomogeneous chemistry.  
243 Although the overall chemical compositions of the particulate matter by these online  
244 methods are useful in determining the total compositions of particles, the results  
245 obtained are more or less similar to those by the bulk analysis methods. In contrast,  
246 offline individual particle analysis represented by SEM-EDX and TEM-EDX can be  
247 used to observe the detailed morphology, internal structure, phase-separated elemental  
248 distribution, mixing states, and all this information can be used to analyze the sources,  
249 secondary chemical reaction and even can be extended to the assessment of climatic  
250 effects and health effects of particulate matter.

### 251 **3 Classifications of atmospheric aerosol individual particles**

252 SEM-EDX and TEM-EDX are the two common methods for individual particle  
253 analysis. In this review, we mainly consider SEM-EDX and TEM-EDX for the  
254 classification of individual particles. Based on EDX analysis and the morphology of  
255 individual particles, atmospheric aerosol individual particles are divided into three  
256 categories, carbonaceous particles, non-carbonaceous particles, and mixed particles.

257 Carbonaceous particles include soot particles, organic particles, and biological particles.  
258 Non-carbonaceous particles include mineral particles, metal particles, fly ash particles,  
259 S-rich (Sulphur-rich) particles, K-rich particles, and sea salt particles (Shi et al., 2003;  
260 Yue et al., 2006; Adachi et al., 2010; Adachi and Buseck, 2011; Li et al., 2010b; Li et  
261 al., 2020a; Dehghani et al., 2017; Liu et al., 2017; Shao et al., 2017; Hou et al., 2018a;  
262 Hu et al., 2018; Abbasi et al., 2019; Wang et al., 2019a; Xing et al., 2020). There are  
263 many types of mixed particles, which will be introduced in the following chapters.

### 264 3.1 Carbonaceous particles

265 Soot particles (Fig. 1a), also known as the major types of particles containing black  
266 carbon (BC) or elemental carbon (EC), are chain-like aggregates (Fig. 1d) containing  
267 spherical carbonaceous particles with sizes ranging from 10 to 100nm (Li et al., 2016b).  
268 Soot particles show onion – like structure at high resolution (Fig. 11a4). Soot particles  
269 (chain-like, cluster-like, and compact-like) are extremely stable under the electron  
270 beam. The soot particles may emission from fossil fuels combustion and biomass  
271 burning (China et al., 2013; Xing et al., 2017). The main element of soot particles is C,  
272 but they can also contain small amounts of O, Si and K. During the aging process, soot  
273 particles can change from chain-like (Fig. 15g) to cluster-like (Fig. 15h), and eventually  
274 become compact-like (Fig. 15i) in shape. Some soot particles also formed core-shell  
275 structure (Fig. 15j) in shape during the aging process.

276 Organic particles (Fig. 2) include Primary Organic Matter (POM) and Secondary  
277 Organic Matter (SOM); often referred to as OM particles. OM particles also include tar  
278 balls. The POM (also known as brown carbon) is spherical or nearly spherical (Fig. 2a,  
279 2d) and extremely stable under the electron beam, and are easily identified under  
280 electron microscopy, with diameters ranging from 30nm-500nm (Posfai et al., 2004;  
281 Posfai et al., 2013a). Secondary organic particles tend to be irregular in shape (Fig 2b),  
282 and often are mixed with secondary sulfate particles. Secondary organic particles can  
283 disintegrate rapidly under the electron beam (Hou et al., 2018a). Organic Particles may  
284 also form core-shell structure in shape after aging (Fig. 2c). Organic particles are mainly

285 derived from fossil fuels and biomass combustion (Li and Shao, 2009a; Posfai and  
286 Buseck, 2010; Liu et al., 2017; Xing et al., 2019). Organic particles are mainly  
287 composed of C and O, and typically contain a small amount of S, Na, Mg, K, and other  
288 trace elements.

289 Biological particles (Fig. 3), also known as bioclasts, generally have specific  
290 morphologies and composition, they include spore (Fig. 3a, 3b), bacteria (Fig. 3c), and  
291 plant debris (Fig. 3d). Biological particles are mainly composed of C, O, P, K and Si  
292 and the size is mainly between 1.8-10 $\mu$ m (Li et al., 2020a).

### 293 3.2 Non-carbonaceous particles

294 Mineral particles (Fig. 4) include long-axis (Fig. 4g), irregular (Fig. 4h) and  
295 regular (Fig. 4i) in shape and are very stable under the electron beam. Mineral particles  
296 can be either anthropogenic or natural and mainly come from construction dust, road  
297 dust and crustal dust. Most mineral particles, often larger than 2 $\mu$ m, originate from the  
298 long-distance transport of sandstorm materials or road-suspended dust (Okada et al.,  
299 2005; Ramírez et al., 2020). Mineral particles are mainly composed of crustal elements,  
300 such as Si, Al, Ca, and Fe (Li and Shao, 2013). The common mineral particles collected  
301 in dust storms or dusty atmospheric conditions are mainly feldspar minerals (Fig. 4a),  
302 clay minerals (Fig. 4b), carbonate minerals (Fig. 4c), sulfate minerals (Fig. 4d), quartz  
303 (Fig. 4e) and unidentified minerals (Fig. 4f). (Wang et al., 2021a).

304 Metal particles (Fig. 5) are sourced from heavy industry, fuel combustion, vehicle  
305 wear, and train track wear (Moreno et al., 2015), and the main elements are Fe (Fig. 5c),  
306 Zn (Fig. 5a), and Pb (Fig. 5b) (Liati et al., 2013). They can exist as pure metal or metal  
307 oxides. The metal particles are not volatile under the electron beam. Metal particles  
308 from combustion-sourced tend to be spherical in shape (Fig. 5c), whereas abrasion-  
309 sourced tend to be more angular.

310 Fly ash particles (Fig. 6a, 6c) are usually spherical in shape and mainly composed  
311 of aluminosilicates (Fig. 6b) with occasional small amounts of Ca, Ti, Mn, and Fe. Fly  
312 ash particles with small particle sizes easily mix with sulfate to form composite particles

313 and rarely exist alone. Coal combustion is a common source of fly ash particles  
314 (Kashiwakura et al., 2010; Wang et al., 2019a), producing non-crystalline (glassy)  
315 particles that can later partially crystallize (Lawson et al., 2020).

316 S-rich particles (Fig. 7a, 7b, 7c) tend to be irregular in shape and can be volatile  
317 under the electron beam, typically forming ‘foam-like’ structure (Fig. 7a). Some S-rich  
318 particles form core-shell structure after aging (Fig. 7b). The composition of shell may  
319 be organic, sulfate, nitrate, and other inorganic salts (Wang et al., 2021b). Sulfate  
320 particles are the most common S-rich particles in the atmosphere. A study reported that  
321 spherical particles dominated the fine mode in urban and marine samples, these  
322 particles were droplets containing ammonium sulfate (Zhang et al., 2000).

323 K-rich particles (Fig. 8) are a commonly used marker for biomass combustion  
324 although coal combustion also contains a small amount of K (Lu et al., 2017; Zhang et  
325 al., 2020a). K-rich particles in the atmosphere are mainly composed of K, N, Cl and S  
326 usually with irregular shapes (Fig. 8b) (Bi et al., 2011; Giordano et al., 2015). When  
327 the main elements of K-rich particles are K and Cl and have a crystalline structure, they  
328 are usually KCl particles (Fig. 8a). Changes in the elemental ratios of Cl/Na and S/Na  
329 in sea-salt particles are expected from the atmospheric reactions of sulfuric and nitric  
330 acids with these particles (McInnes et al., 1994).

331 Sea salt particles (Fig. 9) are mainly sourced from the ocean or evaporated lakes,  
332 and the main elements are Na, Cl and S (Frey et al., 2020). Sea salt particles are stable  
333 under the electron beam and are typically seen with cubic NaCl crystalline morphology  
334 (Fig. 9a, 9b). In certain particle collection devices, the NaCl can dissolve then  
335 recrystallize on the collection substrates (Jones et al., 2001). In some humid coastal  
336 environments, the cubic sea salt crystals tend to form amorphous sea salt particles after  
337 aging (Fig. 9c) (Li et al., 2010a).

### 338 3.3 Mixed particles

339 Particles in the atmosphere often does not exist as a single phase of chemical  
340 composition. For example, due to the high humidity in haze weather, the physical and

341 chemical reaction between particles is more intense than that in non-haze days. Under  
342 these conditions, particles tend to appear in a mixed state (Fig. 10). The mixing state of  
343 particles affects their physical and chemical properties (Zhang et al., 2008), so it is  
344 necessary to understand the make-up of individual mixed particles. Individual particle  
345 analysis has many advantages in the study of these mixed particles, compared to bulk  
346 analysis. The mixing state of individual particle can be divided into internal mixing and  
347 external mixing. External mixing is defined as no contact between particles and no  
348 change in the physical and chemical properties between particles. Internal mixing is  
349 defined as the simultaneous presence of two or more aerosol components in an  
350 individual particle (Li et al., 2016c). The term “mixed particles” used in this review  
351 refers to the internal mixed particles. We divide the internal mixing into heterogeneous  
352 mixing and inhomogeneous mixing. Homogeneous mixing refers to the uniformity of  
353 mixing between particles, indicating a total mixing. Heterogeneous mixing often shows  
354 a mixture of multiple phases of particles, indicating an incomplete mixing. Based on  
355 the morphology and internal structure, the internal mixed particles can be subdivided  
356 into two structural types, that is, irregular mixing shape (Fig. 10a, 10b) and core-shell  
357 structure (Fig. 10d). In terms of chemical compositions, the internal mixed particles  
358 have been divided into the organic and sulfate mixed particles (Fig. 10a), organic and  
359 soot mixed particles (Fig. 10b), organic and K-rich mixed particles (Fig. 10c), S-rich  
360 and fly ash mixed particles (Fig. 10d), S-rich and metal mixed particles (Fig. 10e), S-  
361 rich and mineral mixed particles (Fig. 10f), S-rich and soot mixed particles (Fig. 10g)  
362 and K-rich and metal mixed particle (Fig. 10h) (Table 3) (Fan et al., 2016a; Li et al.,  
363 2016c; Chen et al., 2017a; Zhang et al., 2017; Hou et al., 2018a; Liu et al., 2018; Yu et  
364 al., 2019; Zhang et al., 2018).

#### 365 **4 Source analysis of different types of individual particles**

366 The aim of source apportionment of atmospheric particulate matter is to identify,  
367 either qualitatively or quantitatively, the sources of atmospheric particulate matter to  
368 environmental receptors using chemical, physical, mathematical, or other methods. The



369 results of source apportionment can not only identify the outcomes of differentiated  
370 management and control of key areas and sources at the local level, but also help to  
371 develop fast, scientific, effective, and feasible solutions. When the elemental mixtures  
372 in the particulate matter are complex, traditional bulk analytical methods ignore low  
373 concentrations of toxic and characteristic elements, resulting in errors in the results.  
374 Individual particle analysis can directly observe and characterize properties of  
375 individual particles in relation to their sources, which potentially can provide high  
376 resolution of source apportionment and avoid artifacts or confounding factors.

377         The individual particle analysis observes the morphological characteristics of  
378 individual particles by electron microscopy and the characteristic compositional spectra  
379 observed by EDX, and by these criteria, the possible sources of individual particles can  
380 be classified. According to the Technical Guide for the Source Analysis of Particulate  
381 Matter in the Atmosphere, particulate matter emission sources can be divided into  
382 stationary combustion sources, biomass open combustion sources, industrial process  
383 sources and mobile sources. Among them, the stationary combustion sources include  
384 power generation, industrial, and domestic use (coal, diesel, oil, kerosene, fuel oil,  
385 liquefied petroleum gas, gas, natural gas, and other fuel types). Industrial process  
386 sources include metallurgy, building materials, chemical and many other industries. In  
387 the process of source analysis, the bench experiments are the most direct method to  
388 trace the source of atmospheric particles, and smog chamber experiments are the most  
389 direct method to detect the formation of new particles and atmospheric heterogeneous  
390 reactions.

#### 391 4.1 Fingerprint features of individual aerosol particles

392         Microscopy is a method that allows the probable determination of the source of  
393 particulate matter from the microscopic information of individual particles. Microscopy  
394 is therefore suitable for the analysis of particulates with obvious morphological  
395 characteristics. Individual particle analysis can obtain the type, size, quantity, shape,  
396 color, optical properties, chemical composition, and other characteristics of particles.

397 Individual particle analysis can also be used to visually identify the most likely source  
398 of particulate matter. The bench experiment is to analyze the particles emitted from the  
399 source sample and directly characterize the source of the particles. The results for coal  
400 burning, biomass burning, and vehicle exhaust sources can provide information on the  
401 primary particles in the atmosphere.

#### 402 4.1.1 Coal burning bench experiments

403 Emissions from coal burning is an important source of gaseous and particulate  
404 pollutants in the atmosphere, with fine particles emitted being one of the main causes  
405 of regional haze in China (Jones et al., 2009; Pui et al., 2014). After the State Council  
406 of China issued the “Air Pollution Prevention and Control Action Plan” (APPCAP) on  
407 September 10, 2013 (The State Council of China, 2013), the energy infrastructure  
408 changed with a dramatic decrease in coal consumption; however, domestic coal burning  
409 still contributes a significant amount of PM<sub>2.5</sub> to the atmosphere due to incomplete  
410 combustion and dedust devices (Li et al., 2016c; Li et al., 2020b). Wang et al (2019a)  
411 used a measurement system of an atmospheric dilution chamber in the laboratory to  
412 show that the particulate matter produced by coal combustion mainly includes S-rich  
413 particles (Fig. 11a<sub>1</sub>), mineral particles (Fig. 11a<sub>2</sub>), soot particles (Fig. 11a<sub>3</sub>) and organic  
414 particles (Fig. 11a<sub>5</sub>). In the ignition stage, organic particles accounted for the largest  
415 proportion, up to 66%. In the intense combustion stage, soot particles accounted for the  
416 largest proportion, up to 71%, In the final charcoal burning stage, mineral particles  
417 accounted for the largest proportion, up to 73% (Wang et al., 2019a). Hou et al. (2018b)  
418 also showed that the particles produced by coal burning can be divided into soot  
419 particles, organic particles, mineral particles, sulfate, and metal particles. Related  
420 studies have found that in the combustion of low rank coal the particles emitted are  
421 mainly carbonaceous particles (organic particles and soot particles), while the particles  
422 emitted from high rank coal burning are mainly organic and sulfate mixed particles  
423 (Zhang et al., 2018). Therefore, in the different combustion stages and temperatures the  
424 characteristics of particles are different, also the coal rank will result in different types

425 of particles being emitted.

#### 426 4.1.2 Biomass burning bench experiments

427 Agricultural waste is volumetrically one of the most burned biomasses in the world.  
428 The open burning of agricultural residues is a convenient and inexpensive way to  
429 prepare for the next crop but can lead to serious regional haze events (Tariq et al., 2016).  
430 Biomass combustion emits large numbers of organic particles and gaseous pollutants,  
431 including Non-Methane Volatile Organic Compounds (NMVOCs), CO, CO<sub>2</sub>, CH<sub>4</sub>,  
432 NO<sub>x</sub>, NH<sub>3</sub>, OC, EC and metals (Bond et al., 2004; Li et al., 2007; Chang-Graham et al.,  
433 2011; Heringa et al., 2011; Bond et al., 2013; Laskin et al., 2015). Biomass burning is  
434 also the second largest source of non-methane organic gases in the atmosphere  
435 (Stockwell et al., 2014). Li et al. (2021b) showed that there were mainly five types of  
436 particles in straw burning of corn, wheat and rice. These were soot particles (Fig. 11b<sub>1</sub>),  
437 K-rich particles (Fig. 11b<sub>2</sub>), tar balls (Fig. 11b<sub>3</sub>), organic containing K particles (Fig.  
438 11b<sub>4</sub>) and pure organic particles respectively (Fig. 11b<sub>5</sub>). Organic containing K particles  
439 accounted for the most, followed by organic particles. Soot particles only appear in the  
440 flaming burning stage (Li, 2021). When comparing the particles emitted by coal  
441 burning, it is found that soot particles are greatly reduced, and there are very few S-rich  
442 particles and mineral particles emitted by biomass burning.

#### 443 4.1.3 Vehicle exhaust emissions bench experiments

444 Vehicle exhaust emissions are major sources of airborne particles in the urban  
445 atmosphere (Hwa and Yu, 2014). The secondary aerosol formed by the particles from  
446 motor vehicle exhaust is an important component in the formation of haze (Huang et  
447 al., 2014). Studies have shown that the number of particle emissions of gasoline engines  
448 are usually lower than those from diesel engines (Alves et al., 2015). Xing et al. (2020)  
449 found that GDI (gasoline-direct-injection) engine and PFI (port fuel injection) engine  
450 mainly emitted six types of particles. they were soot particles (Fig. 11c<sub>1</sub>), Ca-rich  
451 particles (Fig. 11c<sub>2</sub>), organic particles (Fig. 11c<sub>3</sub>), S-rich particles (Fig. 11c<sub>4</sub>), Fe-rich

452 (Fig. 11c<sub>5</sub>) and other particles. Soot particles accounted for the highest proportion of  
453 those emitted by GDI engine, and organic particles accounted for the highest proportion  
454 by PFI engine (Fig. 12) (Xing, 2018). Xing et al. (2020) also found that when gasoline  
455 direct-injection engines are in a cold start and acceleration conditions, soot particles  
456 accounted for a greater proportion (Xing et al., 2020).

#### 457 4.2 The formation of secondary particles and heterogeneous reactions

458 Airborne particles can be thought of as suspensions in reaction containers in which  
459 there are numerous chemical and physical processes, such as multiple phase reactions  
460 and gas-particle distributions (Poschl, 2005; Kuwata and Martin, 2012). The  
461 heterogeneous reactions between aerosol particles and trace gases can change the  
462 mixing state of aerosol particles and the composition of those particles, through several  
463 physical and chemical processes (Fuzzi et al., 2006; Zhang et al., 2008; Posfai and  
464 Buseck, 2010). Li et al. (2011) showed that secondary nitrate and sulfate mixed with  
465 soot and sea salt particles could completely change the surface moisture absorption  
466 properties. Recent studies have shown that liquid particles can accelerate the mass  
467 transfer and multiphase reaction of reactive trace gases, promote the formation of  
468 secondary aerosols, and eventually lead to the rapid increase of aerosol mass (Liu et al.,  
469 2019).

470 Core-shell structure was considered as a sign of particle aging (Niu et al., 2011,  
471 2012). The surface of the core can be used as a heterogeneous reaction site for SO<sub>2</sub> and  
472 NO<sub>x</sub> (Ebert et al., 2016). The ratio of core to shell is usually used to measure the degree  
473 of particle aging. The smaller the ratio is, the more aging the particle. Sometimes the  
474 coating thickness of core-shell structure particles can also be used to directly estimate  
475 the degree of particle aging. The greater the coating thickness is, the more aging the  
476 particle. Xu et al. (2019) showed that organic particles with larger particle sizes had a  
477 higher degree of aging than those with smaller particle sizes, and S-rich particles along  
478 the coast showed more indications of aging than those collected in their urban site (Xu  
479 et al., 2019). Hou et al. (2018) showed that the particles in the city are aged than those

480 collected in a local highway tunnel, which was due to the higher solar radiation in the  
481 city. Under solar radiation, photochemical reactions can promote the aging of primary  
482 particles to form large numbers of secondary organic aerosols (Miracolo et al., 2011).  
483 The mixing state and aging process of particulate matter play an important role in  
484 atmospheric circulation, which will have an important impact on the future study of  
485 aerosol impacts on regional and global climate. Smog chamber experiments are an  
486 important method to study the heterogeneous reaction and aging of atmospheric  
487 particles. Details of chamber setups and associated facilities can be found in Deng et  
488 al., (2017) and Liu et al., (2015).

#### 489 4.2.1 Smog chamber experiments; coal burning particles

490 Coal burning emitted large amounts of particles (organic particles, soot particles,  
491 sulfate particles and mineral particles), which is a major source of regional air pollutant  
492  $PM_{2.5}$ . In addition, coal burning also emits gaseous pollutants such as VOCs,  $NO_x$  and  
493  $SO_2$ . These solid and gaseous pollutants can participate in physical and chemical  
494 processes in the atmospheric environment, such as nucleation, condensation,  
495 gas/particle collision, heterogeneous reaction, or multiphase reaction, and form  
496 secondary organic aerosols (SOA). Jaoui et al. (2012) found that  $SO_2$  can promote the  
497 generation of anthropogenic and biological VOCs for SOA, and showed that  
498 heterogeneous reaction is an important way for the transformation of organic  
499 compounds from gas phase to granular phase. The smoke chamber experiments shows  
500 that large numbers of secondary particulate matter are generated in the photochemical  
501 reaction of the flue gas emitted from coal burning. The morphology of soot particles  
502 changed from chain (Fig. 13a) to cluster dense structure (Fig. 13b). The morphology of  
503 organic particles changed from spherical or quasi-spherical (Fig. 13c) to irregular shape  
504 (Fig. 13d, 2c). Some fresh S-rich particles (Fig. 13e) formed core-shell structure in  
505 shape (Fig. 13f) (Li, 2021).

#### 506 4.2.2 Smog chamber experiments; biomass burning particles

507 Aerosol particles emitted by biomass burning have a significant impact on regional  
508 and global atmospheric environment and climate, especially in developing countries,  
509 where crop straw burning emissions aggravate air pollution. Primary particles emitted  
510 from biomass combustion will age in the air, which directly leads to the formation of  
511 secondary particles, thus exacerbating the formation of regional haze. Li et al. (2003)  
512 found that K-rich particles in aerosol emitted by biomass burning would be converted  
513 into  $K_2SO_4$  and  $KNO_3$  in the photochemical reaction. Hennigan et al. (2011) found that  
514 the emission of organic particles from wood burning increased due to photochemical  
515 oxidation reaction. The smog chamber simulation experiment found that the micro  
516 morphology and chemical composition of particles changed after primary particles  
517 aging. It mainly shows that the K-rich particles change from the initial crystal  
518 morphology (Fig. 14a) to the irregular shape of inclusions (Fig. 14c); In terms of  
519 elements, the content of S increased in particles. K-rich particles are mainly KCl  
520 particles in the early stage and are gradually vulcanized in the aging process to form  
521 more  $K_2SO_4$  particles. The aging process of soot particles also observed that during the  
522 aging process, soot particles changed from chain-like (Fig. 14d) to cluster-like (Fig.  
523 15e), and become compact-like (Fig. 15f) in shape (Li, 2021).

#### 524 4.2.3 Smog chamber experiments; vehicle exhaust emission particles

525 Vehicle exhausts emit a large amount of primary particulate matter, which is an  
526 important source of  $PM_{2.5}$  in the atmosphere. However, gaseous pollutants such as  $SO_2$ ,  
527  $NO_x$  and VOCs emitted by motor vehicle exhaust can generate secondary particulate  
528 matter through physical and chemical reactions in the atmospheric environment, and  
529 their contribution to  $PM_{2.5}$  can also not be ignored. The smog chamber experiments  
530 shows that in Beijing urban atmosphere, gasoline vehicle exhaust rapidly (only 3.5  
531 hours) formed large numbers of secondary organic particles, and the primary particles  
532 also aged. The generation of secondary particles and the aging of primary particles are  
533 affected by a variety of factors, among which the more important are the initial

534 concentration of pollutants discharged by gasoline vehicles (including VOCS, NO<sub>x</sub>,  
535 etc.), relative humidity, light intensity, oxidizer (oxidation level) (Ding et al., 2011;  
536 Donahue et al., 2012). The smoke chamber experiment shows that large numbers of  
537 sulfate particles are generated in the photochemical reaction of the flue gas emitted  
538 from vehicle exhaust. The morphology and composition of primary particles emitted  
539 from gasoline vehicles changed after aging (Fig. 15a, 15b, 15c). Soot particles changed  
540 from chain-like (Fig. 15g) to cluster-like (Fig. 15h), and eventually become compact-  
541 like (Fig. 15i) in shape. Some soot particles also change into core-shell structure. The  
542 morphology of organic particles and Ca-rich particles changed from a spherical  
543 structure (Fig. 15d) to a more irregular shape. In terms of elemental composition, the  
544 amount of S element in organic particles and Ca-rich particles increased (Fig. 15f)  
545 (Xing, 2018).

## 546 **5 Applications in the study of climatic change, geochemical cycling, and the human** 547 **health effects**

548 Individual particle analysis technique is widely used as an important method in  
549 characterization of the physical and chemical properties of airborne particles in recent  
550 research. Individual particle analysis can detect particle sources, heterogeneous  
551 reactions, climatic effects, global geochemical cycling effects, and health effects. The  
552 results obtained by individual particle analysis have greatly improved public awareness  
553 of the hazards of particles in the atmosphere.

### 554 5.1 Airborne particles and climatic change

555 Airborne particles can directly or indirectly affect the climate. Large numbers of  
556 anthropogenic sources (such as soot, organic and sulfate particles) and natural sources  
557 (such as dust and sea salt particles) emitted into the atmosphere will absorb and scatter  
558 the incident solar radiation, thus directly changing the energy budget of the Earth-  
559 atmosphere system, and ultimately affecting climate change (Fig. 16) (Wang et al.,  
560 2018; Adam et al., 2021; Mu et al., 2021). In addition, atmospheric particles can also

561 act as Cloud Condensation Nuclei (CCN) to change the cloud optical properties and  
562 lifetime, and indirectly affect the climate (Buseck and Posfai, 1999; Wang et al., 2019b).  
563 Atmospheric particles can also participate in the heterogeneous reaction of ozone to  
564 affect ozone balance and indirectly affect the energy budget of the Earth-atmosphere  
565 system (McNeill, 2017). The radiation effect of atmospheric particles depends on  
566 particle size, spectral distribution, chemical composition, surface characteristics and the  
567 relative humidity of the environment (Penner et al., 1992; Fan et al., 2016b; Zieger et  
568 al., 2017). In addition, the mixing state of particulate matter (Fig. 17) has also an  
569 important impact on climate (Hou, 2017; Wang et al., 2017). When the relative  
570 humidity of the surrounding environment increases, atmospheric particles can display  
571 hygroscopic behavior, which has an important influence on cloud condensation activity  
572 and atmospheric visibility, and can indirectly affect regional or global climate change  
573 (Chen et al., 2012a; Lei et al., 2014).

574 Remote areas at high altitudes are often seen as pristine environments that are  
575 particularly sensitive to climate change and have received much attention from  
576 scientists. Recent research showed that primary brown carbon particles from biomass  
577 burning in South Asia can travel long distances to the high-altitude Himalayas,  
578 contributing significantly to local atmospheric warming and potentially affecting  
579 glacier melting (Yuan et al., 2020). The study of Zhao et al. (2017) on the Tibet Plateau  
580 showed that the direct surface radiative forcing of black carbon ( $-36.0 \text{ Wm}^{-2}$ ) is much  
581 stronger than the typical levels found at lower altitudes and the contribution of black  
582 carbon to the radiative forcing is higher than at lower altitudes.

### 583 5.1.1 Indirect climatic effects and the hygroscopicity of particles

584 When the relative humidity of the atmospheric environment increases, the ability  
585 of atmospheric particles to absorb water is called the hygroscopicity of particles  
586 (Gasparini et al., 2004). The hygroscopic tandem differential mobility analyzer is the  
587 most common method to measure the hygroscopic growth of particles under different  
588 modes (Liu and Zhang, 2010). The hygroscopic behavior of atmospheric particles has



589 a direct or indirect influence on their moisture content, scattering extinction  
590 characteristics, heterogeneous reactions on the particle's surface, cloud condensation  
591 nucleation characteristics, and human health (Chen et al., 2012a; Lei et al., 2014; Chen  
592 et al., 2016). The hygroscopicity of particles will increase the particle size and lead to  
593 the increase of the extinction efficiency factor, which makes up for the effect of the  
594 reduced surface concentration of particles on the reduced visibility (Yang et al., 2018).  
595 The hygroscopicity of atmospheric particles can be expressed by hygroscopicity growth  
596 factor  $HGF = D_{RH}/D_d$ . In this formula,  $D_{RH}$  and  $D_d$  are the particle size of hygroscopic  
597 and dry particles at a certain relative humidity (Wu et al., 2017). Based on Kohler's  
598 theory, Petters and Kreidenweis (2007) proposed an individual parameter  $\kappa$  (Kappa),  
599 which is independent of relative humidity and particle size, to characterize the  
600 hygroscopicity of particles. The study found that the  $\kappa$  value of rural particle collections  
601 was higher than that of urban collections (the  $\kappa$  value of urban sites was around 0.1-0.3,  
602 the rural sites was about 0.15-0.4) (Wang et al., 2017). Cheung et al. (2020) found that  
603 the  $\kappa$  value of cloud condensation nuclei decreased in the early stages of new particle  
604 formation and increased in the later stages of new particle formation. Recent research  
605 shows that when the relative humidity is 90%, the mass ratios of adsorbed water to dry  
606 mineral ranged from 0.0011-0.3080, the hygroscopicity of mineral aerosols depends  
607 largely on the BET surface area of mineral aerosols; the method uses a measurement of  
608 the physisorption of a gas to derive a value of 'surface area' for a sample (Chen et al.,  
609 2020a). In addition, organic matter coating the surface of inorganic salts in the  
610 atmosphere usually inhibits deliquating and hygroscopic growth of inorganic aerosols.  
611 Zhang et al. (2020b) showed that the coating of organic shells would lag the deliquating  
612 point of sodium chloride crystals, with the thicker the organic coating, the more obvious  
613 the hysteresis effect (hysteresis is the dependence of the state of a system on its history).  
614 The organic particles will be oxidized during aging processes, which will increase  
615 the hydrophilic functional groups on the surface of the particles and increase the  
616 hygroscopicity and cloud condensation nuclear activity of the particles (Bougiatioti et  
617 al., 2016; Slade et al., 2017). Smog chamber simulation experiments show that  $SO_2$  in

618 the atmosphere can promote the formation of some organic aerosols and increase the  
619 activity of cloud condensation nuclei (Li et al., 2015). Sea salt particles are an important  
620 component of atmospheric particles in coastal cities. Due to the rapid aging of sea salt  
621 particles in the urban environment, it has an important influence on hygroscopicity and  
622 light scattering (Adachi and Buseck, 2015). Sea salt particles mainly increase the  
623 amount of CCN, thus increasing precipitation. However, for mineral particles, due to  
624 their high heterogeneity, it is difficult to estimate the effect of atmospheric radiative  
625 forcing. Mineral particles can provide an important interface for atmospheric chemical  
626 reactions. Mineral particles play an important role in climate effect because of their  
627 hygroscopic influence on water circulation in the atmosphere and cloud radiation.  
628 Soluble cations ( $\text{Ca}^{2+}$ ,  $\text{Mg}^{2+}$ ,  $\text{Na}^+$  and  $\text{K}^+$ ) on the surface of mineral particles can have  
629 heterogeneous reactions with atmospheric acids such as  $\text{HNO}_3$  or  $\text{HCl}$ . Meanwhile, the  
630 surface of mineral particles can provide a site for the oxidation of  $\text{SO}_2$  to  $\text{H}_2\text{SO}_4$ , all  
631 these processes will increase the water absorption of mineral particles and eventually  
632 form CCN (Karydis et al., 2017). On the other hand, when larger mineral particles form  
633 CCN, they will compete with smaller particles for moisture in the air, which will reduce  
634 supersaturation and cloud droplet formation (Betancourt and Nenes, 2014). Some  
635 mineral particles, such as  $\text{CaCO}_3$ , have low water absorption capacity, but when they  
636 form  $\text{Ca}(\text{NO}_3)_2$  or  $\text{CaCl}_2$  after aging-related reactions in the air, their hygroscopic  
637 capacity increases, and the activity of CCN increases (Tang et al., 2015). The  
638 hygroscopic properties of atmospheric particles contribute to the study of global or  
639 regional climate change.

#### 640 5.1.2 Direct climate effects and atmospheric visibility

641 Particulate matter can cause local and regional environmental deterioration and  
642 adversely affect the lives of people, the most visual of which is the impact on visibility.  
643 The ‘extinction effect’ caused by absorption and scattering of light by atmospheric  
644 particles, especially fine particles, is the main cause of visibility reduction (Tsai, 2005;  
645 Wu et al., 2018; Han et al., 2020; Sun et al., 2020). The light absorption effect of

646 particulate matter is mainly due to black carbon or substances containing black carbon.  
647 The extinction effect of EC was 73.5% in atmospheric particles in the winter in Tianjin  
648 (Xiao et al., 2014). Studies showed that the aerosol absorption in the winter ( $395 \text{ mm}^{-1}$   
649 at 370 nm and  $99 \text{ mm}^{-1}$  at 880 nm, respectively) was about 5-8 times that in the autumn  
650 ( $49 \text{ mm}^{-1}$  at 370nm and  $18 \text{ mm}^{-1}$  at 880 nm, respectively); at all wavelengths (370nm-  
651 950nm), black carbon is the major light-absorbing carbonaceous component (Zhu et al.,  
652 2021). Although most organic aerosol components are known to have a cooling effect  
653 on the global climate, the brown carbon in organic aerosols can absorb shorter  
654 wavelengths of solar radiation and contribute to climate warming (Alexander et al.,  
655 2008). Sulphate particles have ability to force negative light radiation and reduce  
656 temperature (Liu et al., 2009). The optical properties of atmospheric particles contribute  
657 to the study of global or regional climate change.

## 658 5.2 Airborne particles and global geochemical cycling

659 The mobility and high efficiency of the instruments used in individual particle  
660 analysis are a great advantage when collecting samples in remote areas, with the  
661 potential to better identify the global effects of those particles. Atmospheric particles  
662 emitted from urban cities or industrial areas can reach rural areas, remote areas, oceans  
663 and even the Arctic (Fig. 19) due to the capacity of the atmosphere to transport them  
664 over long distances (Jane and Amber 2015). After dry sedimentation or wet  
665 sedimentation, atmospheric particles will participate in biogeochemical cycle  
666 (Mahowald et al., 2018; Luo et al., 2019). It is known that large amounts of mineral  
667 particles are carried into the atmosphere by strong ground winds and transported over  
668 long distances (Adachi et al., 2020; Ono et al., 2020). Long-distance transport of  
669 mineral particles can alter biogeochemical processes on land and in the ocean. Li et al.  
670 (2014) found that pollutants from haze and Asian dust storms can be transported  
671 continental distances. These particles connect the land, atmosphere, and ocean,  
672 affecting regional climate and hydrological and biogeochemical cycles. Many studies  
673 have shown that long-distance dust storms are preserved in ice cores, ocean floor

674 sediments, and peat (Lambert et al., 2008; Le Roux et al., 2012). Large amounts of  
675 anthropogenic particles are now found in areas where there is little human activity. For  
676 example, long-distance transport of light-absorbing carbonaceous aerosols from south  
677 Asia was observed in the snow cover of Himalayan glaciers (Dong et al., 2018). Sea  
678 salt and sulfate particles coated in organic matter have been found in the Arctic (Yu et  
679 al., 2019). Zhao et al. (2019) found that organic matter in Mount Tai (a mountain  
680 located north of the city of Tai'an, and the highest point in Shandong province, China)  
681 was mixed with regional anthropogenic organic matter and biological organic matter  
682 from long-distance atmospheric transport. Analyses of aerosol particles in the Amazon  
683 Basin show differences in the fraction of particles transported over long distances and  
684 from local sources (Adachi et al., 2020). In the process of long-distance transmission,  
685 the acidic gases in the atmosphere, such as SO<sub>2</sub> and NO<sub>2</sub>, are absorbed by the particle  
686 surface due to heterogeneous reaction with the dust particles, and some particles form  
687 a shell structure on the surface and settle on the terrestrial surface (Li and Shao, 2009b).

688       Dissolution of particulate matter transported over long distances has significant  
689 effects on water, soil, plants, biological communities, and climate. Bioaerosol transport  
690 may affect ocean-atmosphere interactions (Yue et al., 2019). Fe particle emissions from  
691 fossil fuels may be transported to remote areas of the ocean and affect the primary  
692 productivity of phytoplankton and the carbon cycle (Pinedo-Gonzalez et al., 2020).  
693 Large numbers of pollutants such as SO<sub>2</sub> discharged into the atmosphere increased the  
694 content of soluble Fe in the air, which was transported to the marine environment over  
695 a long distance, thus increasing the amount of Fe available to marine organisms and  
696 changing biological activities (Li et al., 2017). Zhang et al. (2019) found that N  
697 increased carbon fixation and indirectly offset global warming. Hg adsorbed on  
698 particles can be transported horizontally (long distances) or vertically (deposition) or  
699 incorporated into nutrient chains and transmitted to organisms via food, making  
700 important contributions to root uptake, leaf deposition, and leaf absorption metal  
701 accumulation in plants (Beldowska et al., 2018). Because black carbon particles stay in  
702 the free troposphere for a long time, black carbon particles can be transported from the

703 tropical low troposphere for a long distance and have an impact on the climate in the  
704 far southern hemisphere (Wiedensohler et al., 2018). Research showed that the east  
705 coast of the United States is affected by long-distance particle transport from various  
706 sources throughout the year, which affects the local precipitation rates (Aldhaif et al.,  
707 2020). The global geochemical cycling of individual particles provides important  
708 information for regional haze control, climate effect and health risk assessment

### 709 5.3 Airborne particles and human health effects

710 Long-term exposure to atmospheric pollution increases the risk of diseases of the  
711 respiratory and cardiovascular systems (Fig. 20). According to statistics in 2015,  
712 globally 8.8 million people died due to atmospheric pollution, and the average life  
713 expectancy of humans was reduced by 2.9 years (Lelieveld et al., 2020). There was a  
714 significant correlation between PM<sub>10</sub> mass concentration and mortality, especially from  
715 cardiovascular and respiratory diseases (Cao et al., 2012; Chen et al., 2012b). The  
716 atmosphere contains a variety of toxic and harmful substances, including polycyclic  
717 aromatic hydrocarbons and their derivatives, heavy metals (Zn, Cu, Cd, Cr, Pb, Mn, Tl,  
718 etc.), black carbon particles, asbestos fibers, and radioactive substances. Short term  
719 atmospheric pollution exposure can lead to lung inflammation or lung damage, and  
720 long-term exposure can lead to chronic obstructive pulmonary disease, or even lung  
721 cancer (Xue et al., 2019; Chen et al., 2020b).

722 The degree of harm from atmospheric particles to human health mainly depends  
723 on the particle size, number, and composition (Dockery and Pope, 1994). The smaller  
724 the particle size, the larger the surface area, onto which harmful substances, viruses and  
725 bacteria can be adsorbed (Georgakakou et al., 2016). The composition of the particles  
726 is one of the main pathogenic factors and determines the type of disease. The  
727 concentration of particles and the exposure time determine the inhaled dose by the  
728 human body. The higher the particle concentration, the longer the exposure time, the  
729 greater the harm to the human body. A variety of individual particle types, such as  
730 nanoscale soot particles (Fig. 18c), organic particles (Fig. 2) and metal particles (Fig.

731 5), are all toxic components of PM<sub>2.5</sub> (Dockery and Pope, 1994; Shao et al., 2006a).  
732 Shao et al. (2007) compared the DNA damage caused by soot particles, mineral  
733 particles, fly ash particles and unknown fine particles, and found that soot and unknown  
734 fine particles were important components leading to a raised plasmid DNA damage.  
735 TEM analysis demonstrated that the toxic metal particles rich in Fe, Zn, Pb and Mn are  
736 usually nanometer in size and abundant in the atmosphere (Li et al., 2013a). Studies  
737 have shown that the mixing of particles (Fig. 18) can also convert insoluble metal  
738 oxides into metal ions (Fig. 4b) that can be deposited in the body (Baltrusaitis et al.,  
739 2012). Nano-sized metal particles of Cu in the air may affect neurological diseases, and  
740 soluble Zn in airborne particles can damage lung cells (Richards et al., 1989; Richards,  
741 2003; Manigrasso et al., 2019). Studies have shown that combined exposure to Fe and  
742 black carbon particles induces oxidative damage, cytotoxicity, and pro-inflammatory  
743 responses in the lung (Zhong et al., 2010). Long-term exposure to black carbon may  
744 also lead to increased eye pressure (Manigrasso et al., 2019). The toxicological  
745 properties of atmospheric particles have improved the public's awareness of the risks  
746 presented by atmospheric haze.

## 747 **6 Future research on individual particle analysis; prospects and priorities**

748 Individual particle analysis technology has been used in various research fields of  
749 atmospheric environmental science, showing a huge potential. Individual particle  
750 analysis technology has obtained some exciting research results and opened a new field  
751 for the study of atmospheric environmental science. However, the potential of  
752 individual particle analysis has not been fully exploited, and the application of  
753 individual particle analysis in atmospheric environment science is not systematic.

754 Future research is likely to include the following aspects.

755 1) The optimization of individual particle methodologies and instruments is  
756 always an urgent task, which would allow more advanced and accurate results.  
757 This will enable research on the physical and chemical properties, optical  
758 properties, and environmental effects of atmospheric particulate matter. It will

- 759 be important to standardize manual and automatic methods.
- 760 2) Obtaining large and scientifically vigorous database of individual particle  
761 analysis statistics is critical, including image processing. Currently individual  
762 particle statistical analysis and image processing is very time-consuming  
763 research. It would significantly benefit from improved computer software and  
764 big data idea for automated particle data processing, generating more reliable  
765 statistics and processed imagery.
- 766 3) Further study is required on individual particle source apportionment, especially  
767 with the optimization of electron microscopes to analyze more particles in a  
768 more practical way. This should include establishing more accurate source  
769 apportionment models, refining, and improving dynamic emission inventories,  
770 and improving emission information from key industries. In addition, there is a  
771 critical need to identify sensitive sources that have significant effects on human  
772 health, atmospheric environment, and effective controls.
- 773 4) The role of atmospheric particulate matter on climate is an important issue and  
774 special attention should be paid on the influence and relationship between  
775 particulate matter and a rapidly changing global climate. Key aspects of this  
776 would include: studying the scattering and absorption effects of different  
777 particle types; exploring the effects of particles on solar radiation and the global  
778 heat balance; elucidating the hygroscopicity and heterogeneous reactions of  
779 different types of atmospheric particles; evaluating the process of cloud  
780 condensation nuclei of different particle types. The importance of individual  
781 particle analysis in climate research should be promoted.
- 782 5) It must be understood that this research is interdisciplinary, integrating with  
783 natural science disciplines such as mathematics, physics, chemistry, earth  
784 science, life science and information science. The use of ‘big data’  
785 methodologies is now commonplace, and presents opportunities to  
786 comprehensively study the atmosphere, particulate matter, meteorology, climate,  
787 and health.
- 788

789 **Acknowledgments**

790 This study is supported by the National Natural Science Foundation of China  
791 (Grant No. 42075107, 41175109), the Projects of International Cooperation and  
792 Exchanges NSFC (Grant No. 41571130031), the Fundamental Research Funds for the  
793 Central Universities, and the Yueqi Scholar fund of China University of Mining and  
794 Technology (Beijing).

795



796 **References**

797 Abbasi, S., Keshavarzi, B., Moore, F., Turner, A., Kelly, F.J., Dominguez, A.O.,  
798 Jaafarzadeh, N., 2019. Distribution and potential health impacts of microplastics and  
799 microrubbers in air and street dusts from Asaluyeh County, Iran. *Environ Pollut.* 244,  
800 153-164.

801 Adachi, K., Buseck, P.R., 2011. Atmospheric tar balls from biomass burning in  
802 Mexico. *J Geophys Res-Atmos.* 116, D05204.

803 Adachi, K., Buseck, P.R., 2015. Changes in shape and composition of sea salt  
804 particles upon aging in an urban atmosphere. *Atmos Environ.* 100, 1-9.

805 Adachi, K., Chung, S.H., Buseck, P.R., 2010. Shapes of soot aerosol particles and  
806 implications for their effects on climate. *J Geophys Res-Atmos.* 115, D15206.

807 Adachi, K., Oshima, N., Gong, Z., de Sa, S., Bateman, A.P., Martin, S.T., de Brito,  
808 J.F., Artaxo, P., Cirino, G.G., Sedlacek, A.J., III, Buseck, P.R., 2020. Mixing states of  
809 Amazon basin aerosol particles transported over long distances using transmission  
810 electron microscopy. *Atmos Chem Phys.* 20, 11923-11939.

811 Adam, M.G., Tran, P.T.M., Bolan, N., Balasubramanian, R., 2021. Biomass  
812 burning-derived airborne particulate matter in Southeast Asia: A critical review. *J*  
813 *Hazard Mater.* 407, 124760.

814 Aldhaif, A.M., Lopez, D.H., Dadashazar, H., Sorooshian, A., 2020. Sources,  
815 frequency, and chemical nature of dust events impacting the United States East coast.  
816 *Atmos Environ.* 231, 117456.

817 Alexander, D.T.L., Crozier, P.A., Anderson, J.R., 2008. Brown carbon spheres in  
818 East Asian outflow and their optical properties. *Science.* 321, 833-836.

819 Alves, C.A., Lopes, D.J., Calvo, A.I., Evtyugina, M., Rocha, S., Nunes, T., 2015.  
820 Emissions from light duty diesel and gasoline in use vehicles measured on chassis  
821 dynamometer test cycles. *Aerosol Air Qual Res.* 15, 99-116.

822 Ari, A., Ari, P.E., Gaga, E.O., 2020. Chemical characterization of size segregated  
823 particulate matter by inductively coupled plasma- Tandem mass spectrometry. *Talanta.*  
824 208, 120350.

825 Ayash, T., Gong, S., Jia, C.Q., 2008. Direct and indirect shortwave radiative effects  
826 of sea salt aerosols. *J Climate*. 21, 3207-3220.

827 Ayers, G.P., 1977. An improved thin film sulphate test for submicro particles.  
828 *Atoms Environ*. 11, 391-395.

829 Baltrusaitis, J., Chen, H., Rubasinghege, G., Grassian, V.H., 2012. Heterogeneous  
830 atmospheric chemistry of lead oxide particles with nitrogen dioxide increases lead  
831 solubility: environmental and health implications. *Environ Sci Technol*. 46, 12806-  
832 12813.

833 Beldowska, M., Saniewska, D., Gebka, K., Kwasigroch, U., Korejwo, E., Kobos,  
834 J., 2018. Simple screening technique for determination of adsorbed and absorbed  
835 mercury in particulate matter in atmospheric and aquatic environment. *Talanta*. 182,  
836 340-347.

837 Betancourt, R.M., Nenes, A., 2014. Droplet activation parameterization: the  
838 population splitting concept revisited. *Geosci Model Dev*. 7, 2345-2357.

839 Bi, X., Zhang, G., Li, L., Wang, X., Li, M., Sheng, G., Fu, J., Zhou, Z., 2011.  
840 Mixing state of biomass burning particles by single particle aerosol mass spectrometer  
841 in the urban area of PRD, China. *Atmos Environ*. 45, 3447-3453.

842 Bigg, E.K., Ono, A., Williams, J.A., 1974. Chemical tests for individual  
843 submicron aerosol particles. *Atmos Environ*. 8, 1-13.

844 Bond, T.C., Doherty, S.J., Fahey, D.W., Forster, P.M., Berntsen, T., DeAngelo, B.J.,  
845 Flanner, M.G., Ghan, S., Kaercher, B., Koch, D., Kinne, S., Kondo, Y., Quinn, P.K.,  
846 Sarofim, M.C., Schultz, M.G., Schulz, M., Venkataraman, C., Zhang, H., Zhang, S.,  
847 Bellouin, N., Guttikunda, S.K., Hopke, P.K., Jacobson, M.Z., Kaiser, J.W., Klimont, Z.,  
848 Lohmann, U., Schwarz, J.P., Shindell, D., Storelvmo, T., Warren, S.G., Zender, C.S.,  
849 2013. Bounding the role of black carbon in the climate system: A scientific assessment.  
850 *J Geophys Res-Atmos*. 118, 5380-5552.

851 Bond, T.C., Streets, D.G., Yarber, K.F., Nelson, S.M., Woo, J.H., Klimont, Z., 2004.  
852 A technology-based global inventory of black and organic carbon emissions from  
853 combustion. *J Geophys Res-Atmos*. 109, D14203.

854 Bougiatioti, A., Bezantakos, S., Stavroulas, I., Kalivitis, N., Kokkalis, P., Biskos,  
855 G., Mihalopoulos, N., Papayannis, A., Nenes, A., 2016. Biomass-burning impact on  
856 CCN number, hygroscopicity and cloud formation during summertime in the eastern  
857 Mediterranean. *Atmos Chem Phys*. 16, 7389-7409.

858 Buiarelli, F., Di Filippo, P., Pomata, D., Riccardi, C., Simonetti, G., 2018. A rapid  
859 method for the determination of levoglucosan in NIST standard reference material  
860 1649a by HPLC-MS/MS. *Atmos Environ*. 195, 24-29.

861 Buseck, P.R., Posfai, M., 1999. Airborne minerals and related aerosol particles:  
862 Effects on climate and the environment. *P Natl Acad Sci USA*. 96, 3372-3379.

863 Cao, C., Jiang, W., Wang, B., Fang, J., Lang, J., Tian, G., Jiang, J., Zhu, T.F., 2014.  
864 Inhalable microorganisms in Beijing's PM<sub>2.5</sub> and PM<sub>10</sub> pollutants during a severe smog  
865 event. *Environ Sci Technol*. 48, 1499-1507.

866 Cao, J., Xu, H., Xu, Q., Chen, B., Kan, H., 2012. Fine particulate matter  
867 constituents and cardiopulmonary mortality in a heavily polluted Chinese city. *Environ*  
868 *Health Persp*. 120, 373-378.

869 Chai, G., He, H., Sha, Y., Zhai, G., Zong, S., 2019. Effect of PM<sub>2.5</sub> on daily  
870 outpatient visits for respiratory diseases in Lanzhou, China. *Sci Total Environ*. 649,  
871 1563-1572.

872 Chan, C.K., Yao, X., 2008. Air pollution in megacities in China. *Atmos Environ*.  
873 42, 1-42.

874 Chang Graham, A.L., Profeta, L.T.M., Johnson, T.J., Yokelson, R.J., Laskin, A.,  
875 Laskin, J., 2011. Case study of water soluble metal containing organic constituents of  
876 biomass burning aerosol. *Environ Sci Technol*. 45, 1257-1263.

877 Chen, H., Yang, S., Li, Y., Yin, Y., Zhang, Z., Yu, X., Kang, N., Yan, Q., Xia, H.,  
878 2016. Hygroscopic properties and closure of aerosol chemical composition in Mt.  
879 Huang in summer. *Environ Sci*. 37, 2008-2016. (In Chinese with English abstract)

880 Chen, J., Zhao, C.S., Ma, N., Liu, P.F., Goebel, T., Hallbauer, E., Deng, Z.Z., Ran,  
881 L., Xu, W.Y., Liang, Z., Liu, H.J., Yan, P., Zhou, X.J., Wiedensohler, A., 2012a. A  
882 parameterization of low visibilities for hazy days in the North China Plain. *Atmos Chem*

883 Phys. 12, 4935-4950.

884 Chen, L., Peng, C., Gu, W., Fu, H., Jian, X., Zhang, H., Zhang, G., Zhu, J., Wang,  
885 X., Tang, M., 2020a. On mineral dust aerosol hygroscopicity. *Atmos Chem Phys.* 20,  
886 13611-13626.

887 Chen, R., Kan, H., Chen, B., Huang, W., Bai, Z., Song, G., Pan, G., Grp, C.C.,  
888 2012b. Association of particulate air pollution with daily mortality. *Am J Epidemiol.*  
889 175, 1173-1181.

890 Chen, S., Xu, L., Zhang, Y., Chen, B., Wang, X., Zhang, X., Zheng, M., Chen, J.,  
891 Wang, W., Sun, Y., Fu, P., Wang, Z., Li, W., 2017a. Direct observations of organic  
892 aerosols in common wintertime hazes in North China: insights into direct emissions  
893 from Chinese residential stoves. *Atmos Chem Phys.* 17, 1258-1270.

894 Chen, X., Wang, T., Qiu, X., Que, C., Zhang, H., Zhang, L., Zhu, T., 2020b.  
895 Susceptibility of individuals with chronic obstructive pulmonary disease to air pollution  
896 exposure in Beijing, China: A case-control panel study (COPDB). *Sci Total Environ.*  
897 717, 137285.

898 Chen, Y., Wenger, J.C., Yang, F., Cao, J., Huang, R., Shi, G., Zhang, S., Tian, M.,  
899 Wang, H., 2017b. Source characterization of urban particles from meat smoking  
900 activities in Chongqing, China using single particle aerosol mass spectrometry. *Environ*  
901 *Pollut.* 228, 92-101.

902 Cheng, X., Pu, Y., Gu, R., 2020. Effect of Shanxi pilot emission trading scheme  
903 on industrial soot and dust emissions: A synthetic control method. *Energ Environ-UK.*  
904 31, 461-478.

905 Cheung, H.C., Chou, C.C.K., Lee, C.S.L., Kuo, W.-C., Chang, S.-C., 2020.  
906 Hygroscopic properties and cloud condensation nuclei activity of atmospheric aerosols  
907 under the influences of Asian continental outflow and new particle formation at a  
908 coastal site in eastern Asia. *Atmos Chem Phys.* 20, 5911-5922.

909 Chi, J., Li, W., Zhang, D., Zhang, J., Lin, Y., Shen, X., Sun, J., Chen, J., Zhang, X.,  
910 Zhang, Y., Wang, W., 2015. Sea salt aerosols as a reactive surface for inorganic and  
911 organic acidic gases in the Arctic troposphere. *Atmos Chem Phys.* 15, 11341-11353.

912 China, S., Mazzoleni, C., Gorkowski, K., Aiken, A.C., Dubey, M.K., 2013.  
913 Morphology and mixing state of individual freshly emitted wildfire carbonaceous  
914 particles. *Nat Commun.* 4, 2122.

915 Choi, N.R., Lee, J.Y., Ahn, Y.G., Kim, Y.P., 2020. Determination of atmospheric  
916 amines at Seoul, South Korea via gas chromatography/tandem mass spectrometry.  
917 *Chemosphere.* 258, 127367.

918 Daigle, C.C., Chalupa, D.C., Gibb, F.R., Morrow, P.E., Oberdorster, G., Utell, M.J.,  
919 Frampton, M.W., 2003. Ultrafine particle deposition in humans during rest and exercise.  
920 *Inhal Toxicol.* 15, 539-552.

921 De Bock, L.A., Van Malderen, H., Van Grieken, R.E., 1994. Individual aerosol  
922 particle composition variations in air masses crossing the north sea. *Environ Sci*  
923 *Technol.* 28, 1513-1520.

924 Dehghani, S., Moore, F., Akhbarizadeh, R., 2017. Microplastic pollution in  
925 deposited urban dust, Tehran metropolis, Iran. *Environ Sci Pollut R.* 24, 20360-20371.

926 Deng, W., Liu, T., Zhang, Y., Situ, S., Hu, Q., He, Q., Zhang, Z., Lü, S., Bi, X.,  
927 Wang, X., Boreave, A., George, C., Ding, X., and Wang, X., 2017. Secondary organic  
928 aerosol formation from photo-oxidation of toluene with NO<sub>x</sub> and SO<sub>2</sub>: Chamber  
929 simulation with purified air versus urban ambient air as matrix, *Atmos Environ.* 150,  
930 67–76.

931 Ding, X., Wang, X., Zheng, M., 2011. The influence of temperature and aerosol  
932 acidity on biogenic secondary organic aerosol tracers: Observations at a rural site in the  
933 central Pearl River Delta region, South China. *Atmos Environ.* 45, 1303-1311.

934 Dockery, D.W., Pope, C.A., 3rd, 1994. Acute respiratory effects of particulate air  
935 pollution. *Annu Rev Publ Health.* 15, 107-132.

936 Dockery, D.W., Pope, C.A., 3rd, Xu, X., Spengler, J.D., Ware, J.H., Fay, M.E.,  
937 Ferris, B.G., Jr., Speizer, F.E., 1993. An association between air pollution and mortality  
938 in six U.S. cities. *The New England journal of medicine.* 329, 1753-1759.

939 Donahue, N.M., Henry, K.M., Mentel, T.F., Kiendler-Scharr, A., Spindler, C.,  
940 Bohn, B., Brauers, T., Dorn, H.P., Fuchs, H., Tillmann, R., Wahner, A., Saathoff, H.,

941 Naumann, K.H., Moehler, O., Leisner, T., Mueller, L., Reinnig, M.C., Hoffmann, T.,  
942 Salo, K., Hallquist, M., Frosch, M., Bilde, M., Tritscher, T., Barmet, P., Praplan, A.P.,  
943 DeCarlo, P.F., Dommen, J., Prevot, A.S.H., Baltensperger, U., 2012. Aging of biogenic  
944 secondary organic aerosol via gas-phase OH radical reactions. *P Natl Acad Sci USA*.  
945 109, 13503-13508.

946 Dong, Z., Kang, S., Qin, D., Shao, Y., Ulbrich, S., Qin, X., 2018. Variability in  
947 individual particle structure and mixing states between the glacier-snowpack and  
948 atmosphere in the northeastern Tibetan Plateau. *Cryosphere*. 12, 3877-3890.

949 Ebert, M., Weigel, R., Kandler, K., Guenther, G., Molleker, S., Grooss, J.U., Vogel,  
950 B., Weinbruch, S., Borrmann, S., 2016. Chemical analysis of refractory stratospheric  
951 aerosol particles collected within the arctic vortex and inside polar stratospheric clouds.  
952 *Atmos Chem Phys*. 16, 8405-8421.

953 Fan, J., Shao, L., Hu, Y., Wang, J., Wang, J., Ma, J., 2016a. Classification and  
954 chemical compositions of individual particles at an eastern marginal site of Tibetan  
955 Plateau. *Atmos Pollut Res*. 7, 833-842.

956 Fan, J., Wang, Y., Rosenfeld, D., Liu, X., 2016b. Review of Aerosol Cloud  
957 interactions: mechanisms, significance, and challenges. *J Atmos Sci*. 73, 4221-4252.

958 Frank, E.R., Lodge, J.P., 1967. Morphological identification of air borne particles  
959 with electron microscope. *J Microsc-Oxford*. 6, 449-456.

960 Fraund, M., Park, T., Yao, L., Bonanno, D., Pham, D.Q., Moffet, R.C., 2019.  
961 Quantitative capabilities of STXM to measure spatially resolved organic volume  
962 fractions of mixed organic/inorganic particles. *Atmos Meas Tech*. 12, 1619-1633.

963 Freney, E.J., Adachi, K., Buseck, P.R., 2010. Internally mixed atmospheric aerosol  
964 particles: Hygroscopic growth and light scattering. *J Geophys Res-Atmos*. 115, D19210.

965 Frey, M.M., Norris, S.J., Brooks, I.M., Anderson, P.S., Nishimura, K., Yang, X.,  
966 Jones, A.E., Mastromonaco, M.G.N., Jones, D.H., Wolff, E.W., 2020. First direct  
967 observation of sea salt aerosol production from blowing snow above sea ice. *Atmos*  
968 *Chem Phys*. 20, 2549-2578.

969 Fuzzi, S., Andreae, M.O., Huebert, B.J., Kulmala, M., Bond, T.C., Boy, M.,

970 Doherty, S.J., Guenther, A., Kanakidou, M., Kawamura, K., Kerminen, V.M., Lohmann,  
971 U., Russell, L.M., Poeschl, U., 2006. Critical assessment of the current state of scientific  
972 knowledge, terminology, and research needs concerning the role of organic aerosols in  
973 the atmosphere, climate, and global change. *Atmos Chem Phys*. 6, 2017-2038.

974 Garcia Hernandez, C., Ferrero, A., Estarlich, M., Ballester, F., 2019. Exposure to  
975 ultrafine particles in children until 18 years of age: A systematic review. *Indoor Air*. 30,  
976 7-23.

977 Gard, E., Mayer, J.E., Morrical, B.D., 1997. Real-time analysis of individual  
978 atmospheric aerosol particles: design and performance of a portable ATOFMS. *Anal*  
979 *Chem*. 69, 4083-4091.

980 Gasparini, R., Li, R.J., Collins, D.R., 2004. Integration of size distributions and  
981 size-resolved hygroscopicity measured during the Houston Supersite for compositional  
982 categorization of the aerosol. *Atmos Environ*. 38, 3285-3303.

983 Georgakakou, S., Gourgoulialis, K., Daniil, Z., Bontozoglou, V., 2016. Prediction  
984 of particle deposition in the lungs based on simple modeling of alveolar mixing. *Resp*  
985 *Physiol Neurobi*. 225, 8-18.

986 Ghosal, S., Weber, P.K., Laskin, A., 2014. Spatially resolved chemical imaging of  
987 individual atmospheric particles using nanoscale imaging mass spectrometry: insight  
988 into particle origin and chemistry. *Anal Methods-UK*. 6, 2444-2451.

989 Giordano, M., Espinoza, C., Asa-Awuku, A., 2015. Experimentally measured  
990 morphology of biomass burning aerosol and its impacts on CCN ability. *Atmos Chem*  
991 *Phys*. 15, 1807-1821.

992 Han, L., Sun, Z., He, J., Hao, Y., Tang, Q., Zhang, X., Zheng, C., Miao, S., 2020.  
993 Seasonal variation in health impacts associated with visibility in Beijing, China. *Sci*  
994 *Total Environ*. 730, 139149.

995 He, J., Hu, Q., Jiang, M., Huang, Q., 2021. Nanostructure and reactivity of soot  
996 particles from open burning of household solid waste, *Chemosphere*. 269, 129395.

997 Hennigan, C.J., Miracolo, M.A., Engelhart, G.J., May, A.A., Presto, A.A., Lee, T.,  
998 Sullivan, A.P., McMeeking, G.R., Coe, H., Wold, C.E., Hao, W.M., Gilman, J.B., Kuster,

999 W.C., de Gouw, J., Schichtel, B.A., Collett, J.L., Jr., Kreidenweis, S.M., Robinson, A.L.,  
1000 2011. Chemical and physical transformations of organic aerosol from the photo-  
1001 oxidation of open biomass burning emissions in an environmental chamber. *Atmos*  
1002 *Chem Phys.* 11, 7669-7686.

1003 Heringa, M.F., DeCarlo, P.F., Chirico, R., Tritscher, T., Dommen, J., Weingartner,  
1004 E., Richter, R., Wehrle, G., Prevot, A.S.H., Baltensperger, U., 2011. Investigations of  
1005 primary and secondary particulate matter of different wood combustion appliances with  
1006 a high-resolution time-of-flight aerosol mass spectrometer. *Atmos Chem Phys.* 11,  
1007 5945-5957.

1008 Hou, C., 2017. Study on individual and aging process of individual particle in  
1009 PM<sub>2.5</sub> in highway tunnel and urban Road. Ph D thesis of China University of Mining &  
1010 Technology, Beijing. (In Chinese with English abstract)

1011 Hou, C., Shao, L., Hu, W., Zhang, D., Zhao, C., Xing, J., Huang, X., Hu, M., 2018.  
1012 Characteristics and aging of traffic-derived particles in a highway tunnel at a coastal  
1013 city in southern China. *Sci Total Environ.* 619, 1385-1393.

1014 Hou, C., Shao, L., Hu, W., Zhang, D., Zhao, C., Xing, J., Huang, X., Hu, M., 2018a.  
1015 Characteristics and aging of traffic-derived particles in a highway tunnel at a coastal  
1016 city in southern China. *Sci Total Environ.* 619, 1385-1393.

1017 Hou, C., Shao, L., Zhao, C., Wang, J., Liu, J., Geng, C., 2018b. Characterization  
1018 of coal burning derived individual particles emitted from an experimental domestic  
1019 stove. *J Environ Sci.* 71, 45-55.

1020 Hu, T., Cao, J., Zhu, C., Zhao, Z., Liu, S., Zhang, D., 2018. Morphologies and  
1021 elemental compositions of local biomass burning particles at urban and glacier sites in  
1022 Southeastern Tibetan Plateau: Results from an expedition in 2010. *Sci Total Environ.*  
1023 628, 772-781.

1024 Huang, R.J., Zhang, Y., Bozzetti, C., Ho, K.-F., Cao, J.J., Han, Y., Daellenbach,  
1025 K.R., Slowik, J.G., Platt, S.M., Canonaco, F., Zotter, P., Wolf, R., Pieber, S.M., Bruns,  
1026 E.A., Crippa, M., Ciarelli, G., Piazzalunga, A., Schwikowski, M., Abbaszade, G.,  
1027 Schnelle-Kreis, J., Zimmermann, R., An, Z., Szidat, S., Baltensperger, U., El Haddad,



1028 I., Prevot, A.S.H., 2014. High secondary aerosol contribution to particulate pollution  
1029 during haze events in China. *Nature*. 514, 218-222.

1030 Hwa, M.Y., Yu, T.Y., 2014. Development of real-world driving cycles and  
1031 estimation of emission factors for in use light duty gasoline vehicles in urban areas.  
1032 *Environ Monit Assess*. 186, 3985-3994.

1033 Iwasaka, Y., Yamato, M., Imasu, R., Ono, A., 1988. Transport of Asian dust  
1034 (KOSA) particles; Importance of weak KOSA events on the geochemical cycle of soil  
1035 particles, *Tellus*. 40B, 494-503.

1036 Jones, E.R., Laurent, J.G.C., Young, A.S., MacNaughton, P., Coull, B.A., Spengler,  
1037 J.D., Allen, J.G., 2021. The effects of ventilation and filtration on indoor PM<sub>2.5</sub> in  
1038 office buildings in four countries. *Build Environ*. 200, 107975.

1039 Jane, K., Amber, G., 2015. Tracking long range atmospheric transport of  
1040 contaminants in Arctic regions using lake sediments. *Environmental Contaminants*. 8,  
1041 223-262.

1042 Jaoui, M., Kleindienst, T.E., Offenberg, J.H., Lewandowski, M., Lonneman, W.A.,  
1043 2012. SOA formation from the atmospheric oxidation of 2-methyl-3-buten-2-ol and its  
1044 implications for PM<sub>2.5</sub>. *Atmos Chem Phys*. 12, 2173-2188.

1045 Jones, T., Wlodarczyk, A., Koshy, L., Brown, P., Longyi, S., BeruBe, K., 2009.  
1046 The geochemistry and bioreactivity of fly-ash from coal burning power stations.  
1047 *Biomarkers*. 14, 45-48.

1048 Jones, T.P., Williamson, B.J., BeruBe, K.A., Richards, R.J., 2001. Microscopy and  
1049 chemistry of particles collected on TEOM filters: Swansea, south Wales, 1998-1999.  
1050 *Atmos Environ*. 35, 3573-3583.

1051 Karydis, V.A., Tsimpidi, A.P., Bacer, S., Pozzer, A., Nenes, A., Lelieveld, J., 2017.  
1052 Global impact of mineral dust on cloud droplet number concentration. *Atmos Chem*  
1053 *Phys*. 17, 5601-5621.

1054 Kashiwakura, S., Ohno, H., Matsubae-Yokoyama, K., Kumagai, Y., Kubo, H.,  
1055 Nagasaka, T., 2010. Removal of arsenic in coal fly ash by acid washing process using  
1056 dilute H<sub>2</sub>SO<sub>4</sub> solvent. *J Hazard Mater*. 181, 419-425.

1057           Katrinak, K.A., Anderson, J.R., Buseck, P.R., 1995. Individual particle types in the  
1058 aerosol of phoenix, Arizona. *Environ Sci Technol.* 29, 321-329.

1059           Krishnamohan, K.S., Bala, G., Cao, L., Duan, L., Caldeira, K., 2020. The climatic  
1060 effects of hygroscopic growth of sulfate aerosols in the Stratosphere. *Earths Future.* 8,  
1061 UNSP e2019EF001326.

1062           Kuwata, M., Martin, S.T., 2012. Phase of atmospheric secondary organic material  
1063 affects its reactivity. *P Natl Acad Sci USA.* 109, 17354-17359.

1064           Lambert, F., Delmonte, B., Petit, J.R., Bigler, M., Kaufmann, P.R., Hutterli, M.A.,  
1065 Stocker, T.F., Ruth, U., Steffensen, J.P., Maggi, V., 2008. Dust-climate couplings over  
1066 the past 800,000 years from the EPICA Dome C ice core. *Nature.* 452, 616-619.

1067           Laskin, A., Laskin, J., Nizkorodov, S.A., 2015. chemistry of atmospheric brown  
1068 carbon. *Chem Rev.* 115, 4335-4382.

1069           Lawson, M.J., Prytherch, Z.C., Jones, T.P., Adams, R.A., BeruBe, K.A., 2020.  
1070 Iron-rich magnetic coal fly ash particles induce apoptosis in human bronchial cells.  
1071 *Appl Sci-Basel.* 10, 8363.

1072           Lazzeri, R., Clauser, G., Iacob, E., Lui, A., Tonidandel, G., Anderle, M., 2003.  
1073 ToF-SIMS and XPS characterisation of urban aerosols for pollution studies. *Appl Surf*  
1074 *Sci.* 203, 767-771.

1075           Le Roux, G., Fagel, N., De Vleeschouwer, F., Krachler, M., Debaille, V., Stille, P.,  
1076 Mattielli, N., van der Knaap, W.O., van Leeuwen, J.F.N., Shotyk, W., 2012. Volcano  
1077 and climate driven changes in atmospheric dust sources and fluxes since the Late  
1078 Glacial in Central Europe. *Geology.* 40, 335-338.

1079           Lei, T., Zuend, A., Wang, W.G., Zhang, Y.H., Ge, M.F., 2014. Hygroscopicity of  
1080 organic compounds from biomass burning and their influence on the water uptake of  
1081 mixed organic ammonium sulfate aerosols. *Atmos Chem Phys.* 14, 11165-11183.

1082           Lelieveld, J., Pozzer, A., Poeschl, U., Fnais, M., Haines, A., Muenzel, T., 2020.  
1083 Loss of life expectancy from air pollution compared to other risk factors: a worldwide  
1084 perspective. *Cardiovasc Res.* 116, 1910-1917.

1085           Li, J., Posfai, M., Hobbs, P.V., Buseck, P.R., 2003. Individual aerosol particles

1086 from biomass burning in southern Africa: 2, Compositions and aging of inorganic  
1087 particles. *J Geophys Res-Atmos.* 108, 8484.

1088 Li, K., Sinha, B., Hoppe, P., 2016a. Speciation of nitrogen-bearing species using  
1089 negative and positive secondary ion spectra with nano secondary ion mass spectrometry.  
1090 *Anal Chem.* 88, 3281-3288.

1091 Li, S., Ma.Yan, Zheng, J., Yao, L., Zhou, Y., Wang, Z., 2015. Physicochemical  
1092 properties of secondary organic aerosols and cloud condensation activity in ozone  
1093 oxidation of  $\alpha$ -pinene. *Environ Chem.* 34, 1633-1641. (In Chinese with English abstract)

1094 Li, W., Liu, L., Xu, L., Zhang, J., Yuan, Q., Ding, X., Hu, W., Fu, P., Zhang, D.,  
1095 2020a. Overview of primary biological aerosol particles from a Chinese boreal forest:  
1096 Insight into morphology, size, and mixing state at microscopic scale. *Sci Total Environ.*  
1097 719, 137520.

1098 Li, W., Liu, L., Zhang, J., Xu, L., Wang, Y., Sun, Y. and Shi, Z., 2021. Microscopic  
1099 evidence for phase separation of organic species and inorganic salts in fine ambient  
1100 aerosol particles. *Environ Sci Techn.* 55, 2234-2242.

1101 Li, W., Shao, L., 2009a. Transmission electron microscopy study of aerosol  
1102 particles from the brown hazes in northern China. *J Geophys Res-Atmos.* 114, D09302.

1103 Li, W., Shao, L., 2009b. Observation of nitrate coatings on atmospheric mineral  
1104 dust particles. *Atmos Chem Phys.* 9, 1863-1871.

1105 Li, W., Shao, L., 2010. Characterization of mineral particles in winter fog of  
1106 Beijing analyzed by TEM and SEM. *Environ Monit Assess.* 161, 565-573.

1107 Li, W., Shao, L., Shen, R., Yang, S., Wang, Z., Tang, U., 2011. Internally mixed  
1108 sea salt, soot, and sulfates at macao, a coastal city in South China. *J Air Waste Manage.*  
1109 61, 1166-1173.

1110 Li, W., Shao, L., 2013. Study on Individual Aerosol Particles in Fog, Brown Haze,  
1111 and Dust Storm Episodes. Science Press. Beijing. 146pp.

1112 Li, W., Shao, L., Shi, Z., Chen, J., Yang, L., Yuan, Q., Yan, C., Zhang, X., Wang,  
1113 Y., Sun, J., Zhang, Y., Shen, X., Wang, Z., Wang, W., 2014. Mixing state and  
1114 hygroscopicity of dust and haze particles before leaving Asian continent. *J Geophys*

1115 Res-Atmos. 119, 1044-1059.

1116 Li, W., Shao, L., Wang, W., Li, H., Wang, X., Li, Y., Li, W., Jones, T., Zhang, D.,  
1117 2020b. Air quality improvement in response to intensified control strategies in Beijing  
1118 during 2013-2019. *Sci Total Environ.* 744, 140776.

1119 Li, W., Shao, L., Wang, Z., Shen, R., Yang, S., Tang, U., 2010a. Size, composition,  
1120 and mixing state of individual aerosol particles in a South China coastal city. *J Environ*  
1121 *Sci.* 22, 561-569.

1122 Li, W., Shao, L., Zhang, D., Ro, C.U., Hu, M., Bi, X., Geng, H., Matsuki, A., Niu,  
1123 H., Chen, J., 2016b. A review of single aerosol particle studies in the atmosphere of  
1124 East Asia: morphology, mixing state, source, and heterogeneous reactions. *J Clean Prod.*  
1125 112, 1330-1349.

1126 Li, W., Sun, J., Xu, L., Shi, Z., Riemer, N., Sun, Y., Fu, P., Zhang, J., Lin, Y., Wang,  
1127 X., Shao, L., Chen, J., Zhang, X., Wang, Z., Wang, W., 2016c. A conceptual framework  
1128 for mixing structures in individual aerosol particles. *J Geophys Res-Atmos.* 121, 13784-  
1129 13798.

1130 Li, W., Wang, T., Zhou, S., Lee, S., Huang, Y., Gao, Y., Wang, W., 2013a.  
1131 Microscopic observation of metal-containing particles from Chinese continental  
1132 outflow observed from a non-industrial site. *Environ Sci Technol.* 47, 9124-9131.

1133 Li, W., Xu, L., Liu, X., Zhang, J., Lin, Y., Yao, X., Gao, H., Zhang, D., Chen, J.,  
1134 Wang, W., Harrison, R.M., Zhang, X., Shao, L., Fu, P., Nenes, A., Shi, Z., 2017. Air  
1135 pollution-aerosol interactions produce more bioavailable iron for ocean ecosystems. *Sci*  
1136 *Adv.* 3, e1601749.

1137 Li, W., Shao, L., Buseck, P.R., 2010b. Haze types in Beijing and the influence of  
1138 agricultural biomass burning. *Atmos Chem Phys.* 10, 8119-8130.

1139 Li, X., Wang, S., Duan, L., Hao, J., Li, C., Chen, Y., Yang, L., 2007. Particulate  
1140 and trace gas emissions from open burning of wheat straw and corn stover in China.  
1141 *Environ Sci Technol.* 41, 6052-6058.

1142 Li, Y., 2021. Characteristics and aging process of individual aerosol particles  
1143 emitted from biomass and residential coal combustion. Ph D thesis of China University

1144 of Mining & Technology, Beijing. (In Chinese with English abstract)

1145 Li, Z., Shao, L., Fan, J., Hu, Y., Hou, C., 2013b. Morphology and elemental  
1146 composition of individual particles under different weather conditions in Beijing. *China*  
1147 *Environ Sci.* 33, 1546-1552. (In Chinese with English abstract)

1148 Liati, A., Schreiber, D., Eggenchwiler, P.D., Dasilva, Y.A.R., 2013. Metal particle  
1149 emissions in the exhaust stream of diesel engines: an electron microscope study.  
1150 *Environ Sci Technol.* 47, 14495-14501.

1151 Liu, T., Wang, X., Deng, W., Hu, Q., Ding, X., Zhang, Y., He, Q., Zhang, Z., Lü,  
1152 S., Bi, X., Chen, J., and Yu, J., 2015. Secondary organic aerosol formation from  
1153 photochemical aging of light-duty gasoline vehicle exhausts in a smog chamber. *Atmos*  
1154 *Chem Phys.* 15, 9049–9062.

1155 Liu, X., Jia, H., Qi, J., Zhang, J., Ma, Q., 1994. Scanning electron microscope  
1156 study and pollution source identification of atmospheric particulate matter in Qingdao.  
1157 *Res Environ Sci.* 7, 10-17. (In Chinese with English abstract)

1158 Liu, L., Kong, S., Zhang, Y., Wang, Y., Xu, L., Yan, Q., Lingaswamy, A.P., Shi, Z.,  
1159 Lv, S., Niu, H., Shao, L., Hu, M., Zhang, D., Chen, J., Zhang, X., Li, W., 2017.  
1160 Morphology, composition, and mixing state of primary particles from combustion  
1161 sources - crop residue, wood, and solid waste. *Sci Rep-UK.* 7, 5047.

1162 Liu, L., Zhang, J., Xu, L., Yuan, Q., Huang, D., Chen, J., Shi, Z., Sun, Y., Fu, P.,  
1163 Wang, Z., Zhang, D., Li, W., 2018. Cloud scavenging of anthropogenic refractory  
1164 particles at a mountain site in North China. *Atmos Chem Phys.* 18, 14681-14693.

1165 Liu, X., Zhang, Y., 2010. Advances in research on aerosol hygroscopic properties  
1166 at home and abroad. *Climatic Environ Res.* 6, 806-816. (In Chinese with English  
1167 abstract)

1168 Liu, Y., Sun, J., Yang, B., 2009. The effects of black carbon and sulphate aerosols  
1169 in China regions on East Asia monsoons. *Tellus B.* 61, 642-656.

1170 Liu, Y., Wu, Z., Huang, X., Shen, H., Bai, Y., Qiao, K., Meng, X., Hu, W., Tang,  
1171 M., He, L., 2019. Aerosol phase state and its link to chemical composition and liquid  
1172 water content in a subtropical coastal megacity. *Environ Sci Technol.* 53, 5027-5033.

1173 Lu, S., Tan, Z., Liu, P., Zhao, H., Liu, D., Yu, S., Cheng, P., Win, M.S., Hu, J., Tian,  
1174 L., Wu, M., Yonemochi, S., Wang, Q., 2017. Single particle aerosol mass spectrometry  
1175 of coal combustion particles associated with high lung cancer rates in Xuanwei and  
1176 Fuyuan, China. *Chemosphere*. 186, 278-286.

1177 Luo, X., Bing, H., Luo, Z., Wang, Y., Jin, L., 2019. Impacts of atmospheric  
1178 particulate matter pollution on environmental biogeochemistry of trace metals in soil-  
1179 plant system: A review. *Environ Pollut*. 255, 113138.

1180 Mahowald, N.M., Hamilton, D.S., Mackey, K.R.M., Moore, J.K., Baker, A.R.,  
1181 Scanza, R.A., Zhang, Y., 2018. Aerosol trace metal leaching and impacts on marine  
1182 microorganisms. *Nat Commun*. 9, 2614.

1183 Maji, S., Beig, G., Yadav, R., 2020. Winter VOCs and OVOCs measured with  
1184 PTR-MS at an urban site of India: Role of emissions, meteorology and photochemical  
1185 sources. *Environ Pollut*. 258, 113651.

1186 Mamane, Y., Noll, K.E.J.A.E., 1985. Characterization of large particles at a rural  
1187 site in the eastern United States: Mass distribution and individual particle analysis.  
1188 *Atmos Environ*. 19, 611-622.

1189 Manigrasso, M., Capannesi, G., Rosada, A., Lammardo, M., Ceci, P., Petrucci, A.,  
1190 Avino, P., 2020. Deep inorganic fraction characterization of PM<sub>10</sub>, PM<sub>2.5</sub>, and PM<sub>1</sub> in  
1191 an industrial area located in central Italy by means of instrumental neutron activation  
1192 analysis. *Appl Sci-Basel*. 10, 2532.

1193 Manigrasso, M., Protano, C., Astolfi, M.L., Massimi, L., Avinod, P., Vitali, M.,  
1194 Canepari, S., 2019. Evidences of copper nanoparticle exposure in indoor environments:  
1195 Long term assessment, high resolution field emission scanning electron microscopy  
1196 evaluation, in silico respiratory dosimetry study and possible health implications. *Sci*  
1197 *Total Environ*. 653, 1192-1203.

1198 McInnes, L.M., Covert, D.S., Quinn, P.K., Germani, M.S., 1994. Measurements  
1199 of chloride depletion and sulfur enrichment in individual sea salt particles collected  
1200 from the remote marine boundary layer. *J Geophys Res*. 99, 8257-8268.

1201 McMeeking, G.R., Morgan, W.T., Flynn, M., Highwood, E.J., Turnbull, K.,

1202 Haywood, J., Coe, H., 2011. Black carbon aerosol mixing state, organic aerosols and  
1203 aerosol optical properties over the United Kingdom. *Atmos Chem Phys.* 11, 9037-9052.

1204 McNeill, V.F., 2017. Atmospheric aerosols: clouds, chemistry, and climate, in:  
1205 Prausnitz, J.M. (Ed.). *Annu Rev Chem Biomol.* 8, 427-444.

1206 Meesang, W., Bualert, S., Wonglakorn, P., 2013. Sea salt aerosols: Shortwave  
1207 radiative forcing. *Int J Environ Sci Dev.* 4, 104-106.

1208 Menzel, N., Schramel, P., Wittmaack, K., 2002. Elemental composition of aerosol  
1209 particulate matter collected on membrane filters: A comparison of results by PIXE and  
1210 ICP-AES. *Nucl Instrum Meth B.* 189, 94-99.

1211 Middlebrook, A.M., Murphy, D.M., Lee, S.H., Thomson, D.S., Prather, K.A.,  
1212 Wenzel, R.J., Liu, D.Y., Phares, D.J., Rhoads, K.P., Wexler, A.S., Johnston, M.V.,  
1213 Jimenez, J.L., Jayne, J.T., Worsnop, D.R., Yourshaw, I., Seinfeld, J.H., Flagan, R.C.,  
1214 2003. A comparison of particle mass spectrometers during the 1999 Atlanta Supersite  
1215 Project. *J Geophys Res-Atmos.* 108, 8424.

1216 Miracolo, M.A., Hennigan, C.J., Ranjan, M., Nguyen, N.T., Gordon, T.D., Lipsky,  
1217 E.M., Presto, A.A., Donahue, N.M., Robinson, A.L., 2011. Secondary aerosol  
1218 formation from photochemical aging of aircraft exhaust in a smog chamber. *Atmos*  
1219 *Chem Phys.* 11, 4135-4147.

1220 Moreno, T., Martins, V., Querol, X., Jones, T., BeruBe, K., Cruz Minguillon, M.,  
1221 Amato, F., Capdevila, M., de Miguel, E., Centelles, S., Gibbons, W., 2015. A new look  
1222 at inhalable metalliferous airborne particles on rail subway platforms. *Sci Total Environ.*  
1223 505, 367-375.

1224 Mu, Z., Chen, Q., Zhang, L., Guan, D., Li, H., 2021. Photodegradation of  
1225 atmospheric chromophores: changes in oxidation state and photochemical reactivity.  
1226 *Atmos Chem Phys.* 21, 11581-11591.

1227 Naing, N.N., Lee, H.K., 2020. Microextraction and analysis of contaminants  
1228 adsorbed on atmospheric fine particulate matter: A review. *J Chromatogr A.* 1627,  
1229 461433.

1230 Niu, H., Shao, L., Zhang, D., 2011. Aged status of soot particles during the passage

1231 of a weak cyclone in Beijing. *Atmos Environ.* 45, 2699-2703.

1232 Niu, H., Shao, L., Zhang, D., 2012. Soot particles at an elevated site in eastern  
1233 China during the passage of a strong cyclone. *Sci Total Environ.* 430, 217-222.

1234 Oberdorster, G., Gelein, R.M., Ferin, J., Weiss, B., 1995. Association of particulate  
1235 air pollution and acute mortality: involvement of ultrafine particles? *Inhal Toxicol.* 7,  
1236 111-124.

1237 Oberdorster, G., Sharp, Z., Atudorei, V., Elder, A., Gelein, R., Kreyling, W., Cox,  
1238 C., 2004. Translocation of inhaled ultrafine particles to the brain. *Inhal Toxicol.* 16,  
1239 437-445.

1240 Okada, K., Qin, Y., Kai, K., 2005. Elemental composition and mixing properties  
1241 of atmospheric mineral particles collected in Hohhot, China. *Atmos Res.* 73, 45-67.

1242 Oliveira, M.L.S., Flores, E.M.M., Dotto, G. L., Neckel, A., Silva, L.F.O., 2021.  
1243 Nanomineralogy of mortars and ceramics from the Forum of Caesar and Nerva (Rome,  
1244 Italy): The protagonist of black crusts produced on historic buildings. *J Clean Prod.* 278,  
1245 123982.

1246 Ono, K., Mizushima, Y., Furuya, M., Kunihisa, R., Tsuchiya, N., Fukuma, T., Iwata,  
1247 A., Matsuki, A., 2020. Direct measurement of adhesion force of individual aerosol  
1248 particles by atomic force microscopy. *Atmosphere.* 11, 489.

1249 Peng, L., Li, L., Lin, Q., Li, M., Zhang, G., Bi, X., Wang, X., Sheng, G., 2020.  
1250 Does atmospheric processing produce toxic Pb-containing compounds? A case study in  
1251 suburban Beijing by single particle mass spectrometry. *J Hazard Mater.* 382, 121014.

1252 Penner, J.E., Dickinson, R.E., O'Neill, C.A., 1992. Effects of aerosol from biomass  
1253 burning on the global radiation budget. *Science (New York, N.Y.).* 256, 1432-1434.

1254 Petters, M.D., Kreidenweis, S.M., 2007. A single parameter representation of  
1255 hygroscopic growth and cloud condensation nucleus activity. *Atmos Chem Phys.* 7,  
1256 1961-1971.

1257 Pinedo Gonzalez, P., Hawco, N.J., Bundy, R.M., Armbrust, E.V., Follows, M.J.,  
1258 Cael, B.B., White, A.E., Ferron, S., Karl, D.M., John, S.G., 2020. Anthropogenic Asian  
1259 aerosols provide Fe to the North Pacific Ocean. *P Natl Acad Sci USA.* 117, 27862-



1260 27868.

1261 Pope, C.A., 3rd, Thun, M.J., Namboodiri, M.M., Dockery, D.W., Evans, J.S.,  
1262 Speizer, F.E., Heath, C.W., Jr., 1995. Particulate air pollution as a predictor of mortality  
1263 in a prospective study of U.S. adults. *Am J Resp Crit Care*. 151, 669-674.

1264 Pope, C.A., III, Dockery, D.W., 2006. Health effects of fine particulate air  
1265 pollution: Lines that connect. *J Air Waste Manage*. 56, 709-742.

1266 Poschl, U., 2005. Atmospheric aerosols: Composition, transformation, climate and  
1267 health effects. *Angew Chem Int Edit*. 44, 7520-7540.

1268 Posfai, M., Axisa, D., Tompa, E., Freney, E., Bruintjes, R., Buseck, P.R., 2013a.  
1269 Interactions of mineral dust with pollution and clouds: An individual particle TEM  
1270 study of atmospheric aerosol from Saudi Arabia. *Atmos Res*. 122, 347-361.

1271 Posfai, M., Buseck, P.R., 2010. Nature and climate effects of individual  
1272 tropospheric aerosol particles, in: Jeanloz, R., Freeman, K.H. (Eds.). *Annu Rev Earth*  
1273 *Pl Sc*.38, 17-43.

1274 Posfai, M., Gelencser, A., Simonics, R., Arato, K., Li, J., Hobbs, P.V., Buseck, P.R.,  
1275 2004. Atmospheric tar balls: Particles from biomass and biofuel burning. *J Geophys*  
1276 *Res-Atmos*. 109, D06213.

1277 Posfai, M., Kasama, T., Dunin Borkowski, R.E., 2013b. Biominerals at the  
1278 nanoscale: transmission electron microscopy methods for studying the special  
1279 properties of biominerals, 13th EMU School, Univ Granada, Granada, Spain, 14, 377-  
1280 435.

1281 Prospero, J.M., 1999. Long-range transport of mineral dust in the global  
1282 atmosphere: impact of African dust on the environment of the southeastern United  
1283 States. *P Natl Acad Sci USA*. 96, 3396-3403.

1284 Pui, D.Y.H., Chen, S. C., Zuo, Z., 2014. PM<sub>2.5</sub> in China: Measurements, sources,  
1285 visibility and health effects, and mitigation. *Particuology*. 13, 1-26.

1286 Ramírez, O., da Boit, K., Blanco, E., Silva, L.F.O., 2020. Hazardous thoracic and  
1287 ultrafine particles from road dust in a Caribbean industrial city. *Urban Clim*. 33, 100655.

1288 Ramsden, A.R., Shibaoka, M.J.A.E., 1982. Characterization and analysis of

1289 individual fly ash particles from coal-fired power stations by a combination of optical  
1290 microscopy, electron microscopy and quantitative electron microprobe analysis. *Atmos*  
1291 *Environ.* 16, 2191-2195.

1292 Reyes Villegas, E., Bannan, T., Le Breton, M., Mehra, A., Priestley, M., Percival,  
1293 C., Coe, H., Allan, J.D., 2018. Online chemical characterization of food cooking  
1294 organic aerosols: Implications for source apportionment. *Environ Sci Technol.* 52,  
1295 5308-5318.

1296 Richards, R., 2003. What effects do mineral particles have in the lung? *Mineral*  
1297 *Mag.* 67, 129-139.

1298 Richards, R.J., Atkins, J., Marrs, T.C., Brown, R., Masek, L.J.T., 1989. The  
1299 biochemical and pathological changes produced by the intratracheal instillation of  
1300 certain components of zinc-hexachloroethane smoke. *Toxicol Lett.* 54, 79-88.

1301 Rodriguez, E.S., Perron, M.M.G., Strzelec, M., Proemse, B.C., Bowie, A.R., Paull,  
1302 B., 2020. Analysis of levoglucosan and its isomers in atmospheric samples by ion  
1303 chromatography with electrospray lithium cationisation-triple quadrupole tandem mass  
1304 spectrometry. *J Chromatogr A.* 1610, 460557.

1305 Saikia, B.K., Saikia, J., Rabha, S., Silva, L.F., Finkelman, R., 2018. Ambient  
1306 nanoparticles/nanominerals and hazardous elements from coal combustion activity:  
1307 Implications on energy challenges and health hazards. *Geosci Front.* 9, 863-875.

1308 Shao, L., Hu, Y., Fan, J., Wang, J., Wang, J., Ma, J., 2017. Physicochemical  
1309 characteristics of aerosol particles in the Tibetan Plateau: Insights from TEM-EDX  
1310 analysis. *J Nanosci Nanotechnol.* 17, 6899-6908.

1311 Shao, L., Li, J., Zhao, H., Yang, S., Li, H., Li, W., Jones, T., Sexton, K.,  
1312 Environment, K.B.J.A., 2007. Associations between particle physicochemical  
1313 characteristics and oxidative capacity: An indoor PM<sub>10</sub> study in Beijing, China. *Atmos*  
1314 *Environ.* 41, 5316-5326.

1315 Shao, L., Shi, Z., 2000. Study on inhalable particulate matter in urban atmosphere.  
1316 *Environ Prot.* 1, 24-29. (In Chinese with English abstract)

1317 Shao, L., Shi, Z., Jones, T.P., Li, J., Whittaker, A.G., Berube, K.A., 2006a.

1318 Bioreactivity of particulate matter in Beijing air: Results from plasmid DNA assay. *Sci*  
1319 *Total Environ.* 367, 261-272.

1320 Shao, L., Yang, S., Shi, Z., Lv, S. 2006b. A Study on Physico-Chemistry and  
1321 Bioreactivity of Inhalable Particulates in Urban Air. China Meteorol Press. 209.

1322 Shen, L., Wang, H., Cheng, M., Ji, D., Liu, Z., Wang, L., Gao, W., Yang, Y., Huang,  
1323 W., Zhang, R., Zou, J., Wang, Y., 2021. Chemical composition, water content and size  
1324 distribution of aerosols during different development stages of regional haze episodes  
1325 over the North China Plain. *Atmos Environ.* 245, 118020.

1326 Shen, L., Wang, H., Gao, W., Yang, Y., Huang, W., Wang, L., Zhang, R., Zou, J.,  
1327 Ji, D., Wang, Y., 2020. Real-time physiochemistry of urban aerosols during a regional  
1328 haze episode by a single particle aerosol mass spectrometer: Mixing state, size  
1329 distribution and source apportionment. *Atmos Pollut Res.* 11, 1329-1338.

1330 Shi, Y., Ji, Y., Sun, H., Hui, F., Hu, J., Wu, Y., Fang, J., Lin, H., Wang, J., Duan,  
1331 H., Lanza, M., 2015. Nanoscale characterization of PM<sub>2.5</sub> airborne pollutants reveals  
1332 high adhesiveness and aggregation capability of soot particles. *Sci Rep-UK.* 5, 11232.

1333 Shi, Z.B., Shao, L.Y., Jones, T.P., Whittaker, A.G., Lu, S.L., Berube, K.A., He, T.,  
1334 Richards, R.J., 2003. Characterization of airborne individual particles collected in an  
1335 urban area, a satellite city and a clean air area in Beijing, 2001. *Atmos Environ.* 37,  
1336 4097-4108.

1337 Silva, L.F.O., Santosh, M., Schindler, M., Gasparotto, J., Dotto, G.L., Oliveira,  
1338 M.L.S., Hochella, M.F., 2021. Nanoparticles in fossil and mineral fuel sectors and their  
1339 impact on environment and human health: A review and perspective. *Gondwana Res.*  
1340 92, 184-201.

1341 Singh, N., Banerjee, T., Raju, M.P., Deboudt, K., Sorek-Hamer, M., Singh, R.S.,  
1342 Mall, R.K., 2018. Aerosol chemistry, transport, and climatic implications during  
1343 extreme biomass burning emissions over the Indo-Gangetic Plain. *Atmos Chem Phys.*  
1344 18, 14197-14215.

1345 Slade, J.H., Shiraiwa, M., Arangio, A., Su, H., Poeschl, U., Wang, J., Knopf, D.A.,  
1346 2017. Cloud droplet activation through oxidation of organic aerosol influenced by

1347 temperature and particle phase state. *Geophys Res Lett.* 44, 1583-1591.

1348 Stockwell, C.E., Yokelson, R.J., Kreidenweis, S.M., Robinson, A.L., Demott, P.J.,  
1349 Sullivan, R.C., Reardon, J., Ryan, K.C., Griffith, D.W.T., Stevens, L., 2014. Trace gas  
1350 emissions from combustion of peat, crop residue, domestic biofuels, grasses, and other  
1351 fuels: configuration and Fourier transform infrared (FTIR) component of the fourth Fire  
1352 Lab at Missoula Experiment (FLAME-4). *Atmos Chem Phys.* 14, 9727-9754.

1353 Sun, X., Zhao, T., Liu, D., Gong, S., Xu, J., Ma, X., 2020. Quantifying the  
1354 influences of PM<sub>2.5</sub> and relative humidity on change of atmospheric visibility over  
1355 recent winters in an urban area of east China. *Atmosphere.* 11, 461.

1356 Sun, Z., Duan, F., He, K., Du, J., Zhu, L., 2019. Sulfate-nitrate-ammonium as  
1357 double salts in PM<sub>2.5</sub>: Direct observations and implications for haze events. *Sci Total*  
1358 *Environ.* 647, 204-209.

1359 Tang, X., Zhang, Y., Shao, M., 2006. *Atmospheric environmental chemistry (2nd*  
1360 *Edition)*. Higher education press. 4, 739.

1361 Tang, M.J., Whitehead, J., Davidson, N.M., Pope, F.D., Alfarra, M.R., McFiggans,  
1362 G., Kalberer, M., 2015. Cloud condensation nucleation activities of calcium carbonate  
1363 and its atmospheric ageing products. *Phys Chem Chem Phys.* 17, 32194-32203.

1364 Tariq, S., Ul Haq, Z., Ali, M., 2016. Satellite and ground-based remote sensing of  
1365 aerosols during intense haze event of October 2013 over Lahore, Pakistan. *Asia-Pac J*  
1366 *Atmos Sci.* 52, 25-33.

1367 Tervahattu, H., Juhanaja, J., Kupiainen, K., 2002. Identification of an organic  
1368 coating on marine aerosol particles by TOF-SIMS. *J Geophys Res-Atmos.* 107, 4319.

1369 The State Council of China, 2013. Air pollution prevention and control action plan.  
1370 (Accessed 12 September 2013) (In Chinese).

1371 Toner, S.M., Sodeman, D.A., Prather, K.A., 2006. Single particle characterization  
1372 of ultrafine and accumulation mode particles from heavy duty diesel vehicles using  
1373 aerosol time-of-flight mass spectrometry. *Environ Sci Technol.* 40, 3912-3921.

1374 Toner, S.M., Shields, L.G., Sodeman, D.A., Prather, K.A., 2008. Using mass  
1375 spectral source signatures to apportion exhaust particles from gasoline and diesel

1376 powered vehicles in a freeway study using UF-ATOFMS. *Atmos Environ.* 42, 568-581.

1377 Trejos, E.M., Silva, L.F.O., Hower, J.C., Flores, E.M., Gonzalez, C.M., Pachon,  
1378 J.E., Aristizabal, B.H., 2021. Volcanic emissions and atmospheric pollution: A study of  
1379 nanoparticles. *Geosci Front.* 12, 746-755.

1380 Tsai, Y.I., 2005. Atmospheric visibility trends in an urban area in Taiwan 1961-  
1381 2003. *Atmos Environ.* 39, 5555-5567.

1382 Wang, M.J., Zheng, N., Zhao, D.F., Shang, J., Zhu, T., 2021b. Using micro-Raman  
1383 spectroscopy to investigate chemical composition, mixing states, and heterogeneous  
1384 reactions of individual atmospheric particles. *Environ Sci Technol.* 55, 10243-10254

1385 Wang, J., Zhang, Q., Chen, M., Collier, S., Zhou, S., Ge, X., Xu, J., Shi, J., Xie,  
1386 C., Hu, J., Ge, S., Sun, Y., Coe, H., 2017. First chemical characterization of refractory  
1387 black carbon aerosols and associated coatings over the Tibetan Plateau (4730 m a.s.l.).  
1388 *Environ Sci Technol.* 51, 14072-14082.

1389 Wang, Q., Cao, J., Han, Y., Tian, J., Zhang, Y., Pongpiachan, S., Zhang, Y., Li, L.,  
1390 Niu, X., Shen, Z., Zhao, Z., Tipmanee, D., Bunsomboonsakul, S., Chen, Y., Sun, J.,  
1391 2018. Enhanced light absorption due to the mixing state of black carbon in fresh  
1392 biomass burning emissions. *Atmos Environ.* 180, 184-191.

1393 Wang, W., 2020. Individual particle types and aging characteristics of PM<sub>2.5</sub> under  
1394 different pollution weather in Beijing. Ph D thesis of China University of Mining &  
1395 Technology, Beijing. (In Chinese with English abstract)

1396 Wang, W., Shao, L., Li, J., Chang, L., Zhang, D., Zhang, C., Jiang, J., 2019a.  
1397 Characteristics of individual particles emitted from an experimental burning chamber  
1398 with coal from the lung cancer area of Xuanwei, China. *Aerosol Air Qual Res.* 19, 355-  
1399 363.

1400 Wang, W., Shao, L., Zhang, D., Li, Y., Li, W., Liu, P., Xing, J., 2021a.  
1401 Mineralogical similarities and differences of dust storm particles at Beijing from deserts  
1402 in the north and northwest. *Sci Total Environ.* 803, 149980.

1403 Wang, Y., Niu, S., Lv, J., Lu, C., Xu, X., Wang, Y., Ding, J., Zhang, H., Wang, T.,  
1404 Kang, B., 2019b. A new method for distinguishing unactivated particles in cloud

1405 condensation nuclei measurements: Implications for aerosol indirect effect evaluation.  
1406 *Geophys Res Lett.* 46, 14185-14194.

1407 Wang, Y., Wu, Z., Hu, M., 2017. Hygroscopic characteristics of submicron  
1408 particles under different atmospheric conditions in China. *China Environ Sci.* 5, 1601-  
1409 1609. (In Chinese with English abstract)

1410 Wang, Z., Hu, W., Niu, H., Hu, W., Wu, Y., Wu, L., Ren, L., Deng, J., Guo, S., Wu,  
1411 Z., Zhang, D., Fu, P., Hu, M., 2021b. Variations in physicochemical properties of  
1412 airborne particles during a heavy haze-to-dust episode in Beijing. *Sci Total Environ.*  
1413 762, 143081.

1414 Wiedensohler, A., Andrade, M., Weinhold, K., Mueller, T., Birmili, W., Velarde, F.,  
1415 Moreno, I., Forno, R., Sanchez, M.F., Laj, P., Ginot, P., Whiteman, D.N., Krejci, R.,  
1416 Sellegri, K., Reichler, T., 2018. Black carbon emission and transport mechanisms to the  
1417 free troposphere at the La Paz/El Alto (Bolivia) metropolitan area based on the Day of  
1418 Census (2012). *Atmos Environ.* 194, 158-169.

1419 Wu, J., Cheng, W., Lu, H., Shi, Y., He, Y., 2018. The effect of particulate matter  
1420 on visibility in hangzhou, China. *J Environ Sci Manag.* 21, 100-109.

1421 Wu, Z., Zheng, J., Wang, Y., Shang, D., Du, Z., Zhang, Y., Hu, M., 2017. Chemical  
1422 and physical properties of biomass burning aerosols and their CCN activity: A case  
1423 study in Beijing, China. *Sci Total Environ.* 579, 1260-1268.

1424 Xiao, S., Wang, Q.Y., Cao, J.J., Huang, R.J., Chen, W.D., Han, Y.M., Xu, H.M.,  
1425 Liu, S.X., Zhou, Y.Q., Wang, P., Zhang, J.Q., Zhan, C.L., 2014. Long term trends in  
1426 visibility and impacts of aerosol composition on visibility impairment in Baoji, China.  
1427 *Atmos Res.* 149, 88-95.

1428 Xing, J., 2018. Study on characteristics and aging mechanism of individual  
1429 particles in PM<sub>2.5</sub> from Motor vehicle emission. Ph D thesis of China University of  
1430 Mining & Technology, Beijing. (In Chinese with English abstract)

1431 Xing, J., Shao, L., Zhang, W., Peng, J., Wang, W., Hou, C., Shuai, S., Hu, M.,  
1432 Zhang, D., 2019. Morphology and composition of particles emitted from a port fuel  
1433 injection gasoline vehicle under real-world driving test cycles. *J Environ Sci.* 76, 339-

1434 348.

1435 Xing, J., Shao, L., Zhang, W., Peng, J., Wang, W., Shuai, S., Hu, M., Zhang, D.,  
1436 2020. Morphology and size of the particles emitted from a gasoline direct injection  
1437 engine vehicle and their ageing in an environmental chamber. *Atmos Chem Phys.* 20,  
1438 2781-2794.

1439 Xing, J., Shao, L., Zheng, R., Peng, J., Wang, W., Guo, Q., Wang, Y., Qin, Y., Shuai,  
1440 S., Hu, M., 2017. Individual particles emitted from gasoline engines: Impact of engine  
1441 types, engine loads and fuel components. *J Clean Prod.* 149, 461-471.

1442 Xu, L., Zhang, D., Li, W., 2019. Microscopic comparison of aerosol particles  
1443 collected at an urban site in North China and a coastal site in Japan. *Sci Total Environ.*  
1444 669, 948-954.

1445 Xue, T., Liu, J., Zhang, Q., Geng, G., Zheng, Y., Tong, D., Liu, Z., Guan, D., Bo,  
1446 Y., Zhu, T., He, K., Hao, J., 2019. Rapid improvement of PM<sub>2.5</sub> pollution and associated  
1447 health benefits in China during 2013-2017. *Sci China Earth Sci.* 62, 1847-1856.

1448 Yamato, M., Tanaka, H.J.J.o.G.R.A., 1994. Aircraft observations of aerosols in the  
1449 free marine troposphere over the North Pacific Ocean: Particle chemistry in relation to  
1450 air mass origin. *J Geophys Res-Atmos.* 99, 5353-5377.

1451 Yang, S., Yu, X., Zhao, X., Li, Y., Shun, H., Tian, Z., Li, Y., Wu, S., Wang, Z., 2018.  
1452 Characteristics of key size spectrum of PM<sub>2.5</sub> affecting winter haze pollution in taiyuan.  
1453 *Environmental Science.* 39, 2512-2520.

1454 Yu, H., Li, W., Zhang, Y., Tunved, P., Dall'Osto, M., Shen, X., Sun, J., Zhang, X.,  
1455 Zhang, J., Shi, Z., 2019. Organic coating on sulfate and soot particles during late  
1456 summer in the Svalbard Archipelago. *Atmos Chem Phys.* 19, 10433-10446.

1457 Yuan, Q., Wan, X., Cong, Z., Li, M., Liu, L., Shu, S., Liu, R., Xu, L., Zhang, J.,  
1458 Ding, X., Li, W., 2020. In situ observations of light absorbing carbonaceous aerosols at  
1459 Himalaya: Analysis of the South Asian sources and Trans-Himalayan Valleys transport  
1460 pathways. *J Geophys Res-Atmos.* 125, e2020JD032615.

1461 Yuan, Q., Xu, J., Wang, Y., Zhang, X., Pang, Y., Liu, L., Bi, L., Kang, S., Li, W.,  
1462 2019. Mixing state and fractal dimension of soot particles at a remote site in the

1463 Southeastern Tibetan Plateau. *Environ Sci Technol.* 53, 8227-8234.

1464 Yuan, Q., Xu, J.Z., Liu, L., Zhang, A.X., Liu, Y.M., Zhang, J., Wan, X., Li, M.M.,  
1465 Qin, K., Cong, Z.Y., Wang, Y.H., Kang, S.C., Shi, Z.B., Posfai, M., Li, W.J., 2021.  
1466 Evidence for large amounts of brown carbonaceous tarballs in the Himalayan  
1467 atmosphere. *Environ Sci Tech Let.* 8, 16-23.

1468 Yue, S., Ren, L., Song, T., Li, L., Xie, Q., Li, W., Kang, M., Zhao, W., Wei, L.,  
1469 Ren, H., Sun, Y., Wang, Z., Ellam, R.M., Liu, C.Q., Kawamura, K., Fu, P., 2019.  
1470 Abundance and diurnal trends of fluorescent bioaerosols in the troposphere over Mt.  
1471 Tai, China, in Spring. *J Geophys Res-Atmos.* 124, 4158-4173.

1472 Yue, W., Lia, X., Liu, J., Li, Y., Yu, X., Deng, B., Wan, T., Zhang, G., Huang, Y.,  
1473 He, W., Hua, W., Shao, L., Li, W., Yang, S., 2006. Characterization of PM<sub>2.5</sub> in the  
1474 ambient air of Shanghai city by analyzing individual particles. *Sci Total Environ.* 368,  
1475 916-925.

1476 Zalakeviciute, R., Alexandrino, K., Rybarczyk, Y., Debut, A., Vizuete, K., Diaz,  
1477 M., 2020. Seasonal variations in PM<sub>10</sub> inorganic composition in the Andean City. *Sci*  
1478 *Rep-UK.* 10, 17049.

1479 Zhang, D.Z., Zhao, C.S., Qing, Y., 1998. Analysis of composition and morphology  
1480 of dust particles. *Acta Scientiae Circumstantiae.* 18, 3-10. (In Chinese with English  
1481 abstract)

1482 Zhang, D.Z., Shi, G.Y., Iwasaka, Y., Hu, M., 2000. Mixture of sulfate and nitrate  
1483 in coastal atmospheric aerosols: individual particle studies in Qingdao (36 degrees 04 '  
1484 N, 120 degrees 21 ' E), China. *Atmos Environ.* 34, 2669-2679.

1485 Zhang, J., Liu, L., Wang, Y., Ren, Y., Wang, X., Shi, Z., Zhang, D., Che, H., Zhao,  
1486 H., Liu, Y., Niu, H., Chen, J., Zhang, X., Lingaswamy, A.P., Wang, Z., Li, W., 2017.  
1487 Chemical composition, source, and process of urban aerosols during winter haze  
1488 formation in Northeast China. *Environ Pollut.* 231, 357-366.

1489 Zhang, J., Liu, L., Xu, L., Lin, Q., Zhao, H., Wang, Z., Guo, S., Hu, M., Liu, D.,  
1490 Shi, Z., Huang, D., Li, W., 2020a. Exploring wintertime regional haze in northeast  
1491 China: role of coal and biomass burning. *Atmos Chem Phys.* 20, 5355-5372.



1492 Zhang, R., Khalizov, A.F., Pagels, J., Zhang, D., Xue, H., McMurry, P.H., 2008.  
1493 Variability in morphology, hygroscopicity, and optical properties of soot aerosols  
1494 during atmospheric processing. *P Natl Acad Sci USA*. 105, 10291-10296.

1495 Zhang, S., Xu, L., Guo, X., Huang, D., Li, W., 2020b. Effects of secondary organic  
1496 aerosol shells on the hygroscopicity of sodium chloride nuclei: Based on a single  
1497 particle microscale. *Environ Sci*. 41, 2017-2025. (In Chinese with English abstract)

1498 Zhang, Y., Yuan, Q., Huang, D., Kong, S., Zhang, J., Wang, X., Lu, C., Shi, Z.,  
1499 Zhang, X., Sun, Y., Wang, Z., Shao, L., Zhu, J., Li, W., 2018. Direct observations of  
1500 fine primary particles from residential coal burning: insights into their morphology,  
1501 composition, and hygroscopicity. *J Geophys Res-Atmos*. 123, 12964-12979.

1502 Zhao, W., Fu, P., Yue, S., Li, L., Xie, Q., Zhu, C., Wei, L., Ren, H., Li, P., Li, W.,  
1503 Sun, Y., Wang, Z., Kawamura, K., Chen, J., 2019. Excitation emission matrix  
1504 fluorescence, molecular characterization and compound-specific stable carbon isotopic  
1505 composition of dissolved organic matter in cloud water over Mt. Tai. *Atmos Environ*.  
1506 213, 608-619.

1507 Zhao, Z., Wang, Q., Xu, B., Shen, Z., Huang, R., Zhu, C., Su, X., Zhao, S., Long,  
1508 X., Liu, S., Cao, J., 2017. Black carbon aerosol and its radiative impact at a high-altitude  
1509 remote site on the southeastern Tibet Plateau. *J Geophys Res-Atmos*. 122, 5515-5530.

1510 Zhong, C., Zhou, Y., Smith, K.R., Kennedy, I.M., Chen, C., Aust, A.E., Pinkerton,  
1511 K.E., 2010. Oxidative injury in the lungs of neonatal rats following short term exposure  
1512 to ultrafine iron and soot particles. *J Toxicol Env Heal A*. 73, 837-847.

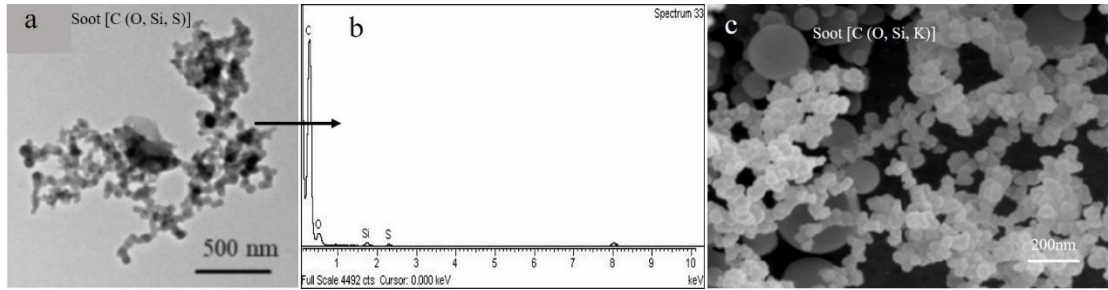
1513 Zhu, C., Qu, Y., Zhou, Y., Huang, H., Liu, H., Yang, L., Wang, Q., Hansen, A.D.A.,  
1514 Cao, J., 2021. High light absorption and radiative forcing contributions of primary  
1515 brown carbon and black carbon to urban aerosol. *Gondwana Res*. 90, 159-164.

1516 Zieger, P., Vaisanen, O., Corbin, J.C., Partridge, D.G., Bastelberger, S., Mousavi  
1517 Fard, M., Rosati, B., Gysel, M., Krieger, U.K., Leck, C., Nenes, A., Riipinen, I.,  
1518 Virtanen, A., Salter, M.E., 2017. Revising the hygroscopicity of inorganic sea salt  
1519 particles. *Nat Commun*. 8, 15883.

1520

1521 **Figure Captions**

1522

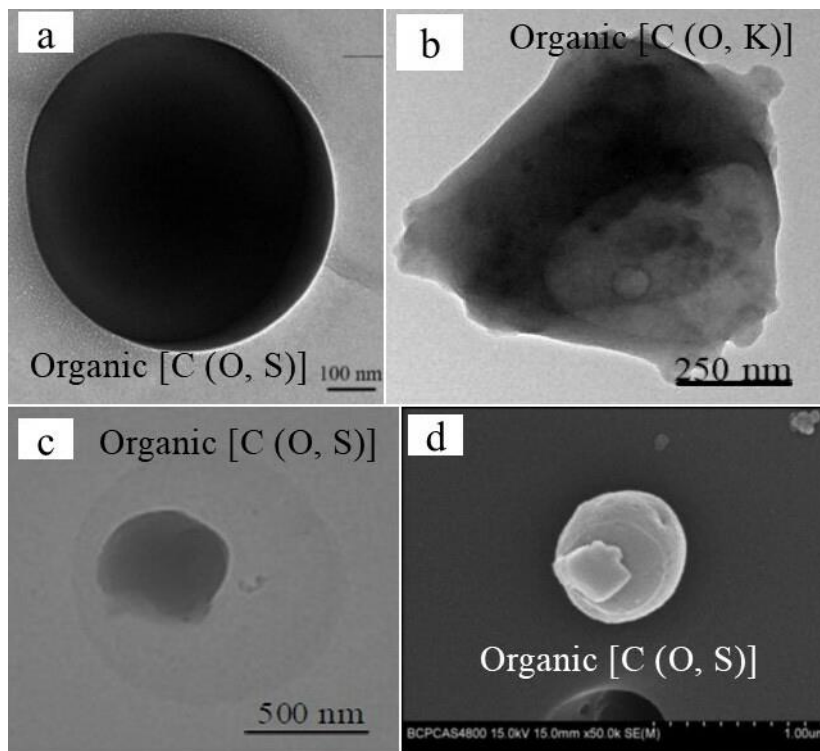


1523

1524 **Figure 1.** Electron microscopy images of soot particles. a Soot particles observed under  
1525 TEM, from PM<sub>2.5</sub> collected in Beijing air 2016. b EDX spectrum of individual soot  
1526 particle shown in a, c Soot particle observed in SEM, from PM<sub>10</sub> collected at a coal  
1527 burning site in Beijing, 2001. a and b are from Wang (2020) and c is from Shao et al.  
1528 (2006b).

1529

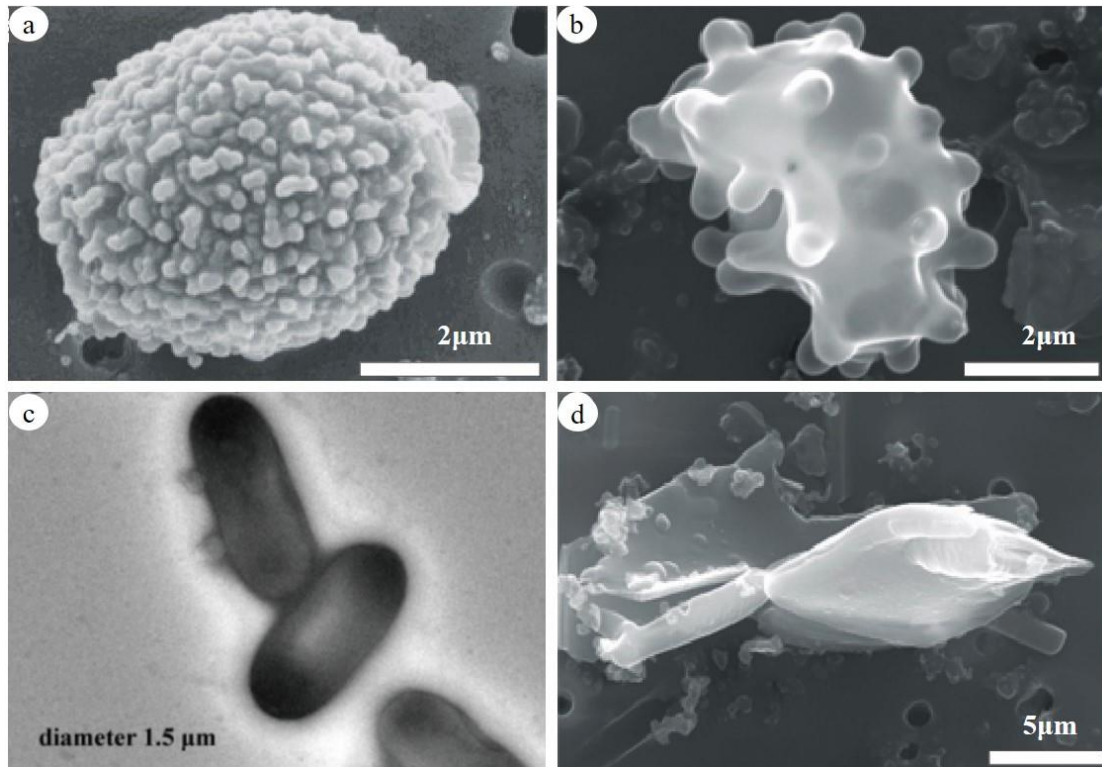
1530



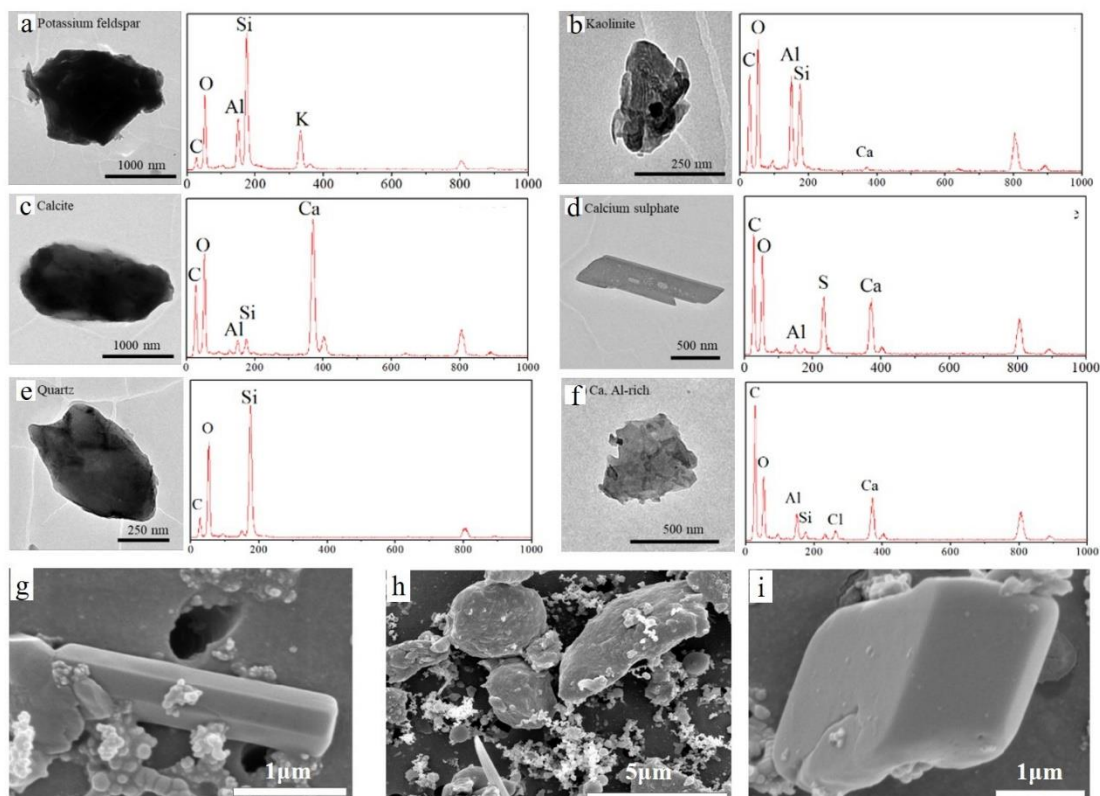
1531

1532 **Figure 2.** Electron microscopy images of organic particles. a Organic particle (TEM)  
1533 from PM<sub>2.5</sub> collected in a tunnel environment in Shenzhen 2014, b Organic particle with  
1534 irregular shape (TEM) from PM<sub>2.5</sub> collected in winter in Beijing, c Organic particle in

1535 core-shell structure (TEM) from PM<sub>2.5</sub> collected in tunnel environment in Shenzhen  
1536 2014, d Organic particles in core shell structure shape (SEM) from PM<sub>2.5</sub> collected in  
1537 winter in Beijing. a and d are from Hou (2017) and b and c are from Wang (2020).  
1538  
1539



1540  
1541 **Figure 3.** SEM images of biological particles. a. b spores, c bacteria, d plant debris.  
1542 The images of a, b and d were from samples collected in Beijing in summer 2001  
1543 (Shao et al., 2006b, reproduced with permission) and c was from PM<sub>2.5</sub> collected in  
1544 the Lesser Khingan Mountain boreal forest of China (Li et al., 2020a, reproduced with  
1545 permission).

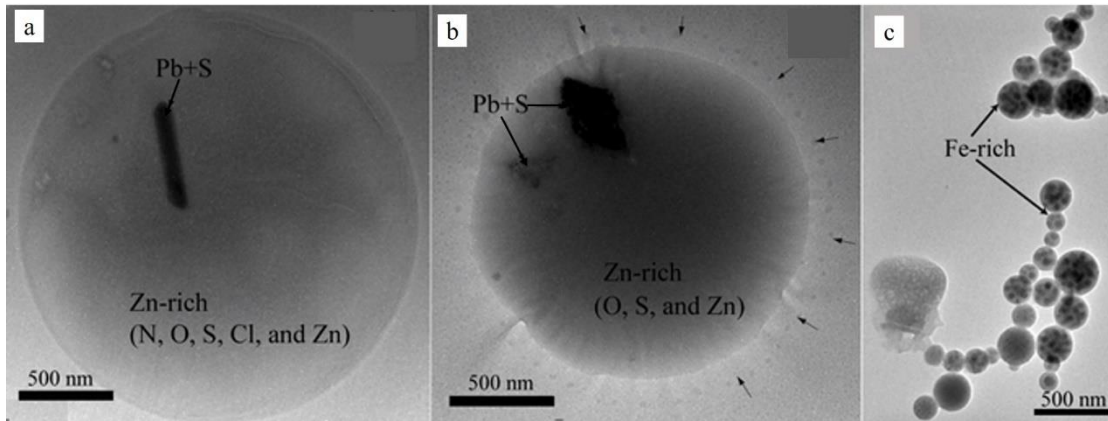


1546

1547 **Figure 4.** Electron microscopy images of mineral particles. a, Potassium feldspar  
 1548 mineral (TEM), b Kaolinite mineral (TEM), c Calcite mineral (TEM), d Calcium  
 1549 sulphate mineral (TEM), e Quartz mineral (TEM), f Ca, Al-rich mineral (TEM), g  
 1550 Mineral particle in Long-axis shape (SEM), h Mineral particle in irregular shape (SEM),  
 1551 i Mineral particle in regular shape. The images a-f were from PM<sub>2.5</sub> samples collected  
 1552 in Beijing during two severe dust storms in spring 2015. The images g-i were from  
 1553 PM<sub>10</sub> samples collected in Beijing in summer 2001. a, b, c, d, e, and f, are from Wang  
 1554 et al. (2021a, reproduced with permission) and g, h and i are from Shao et al. (2006b).

1555

1556

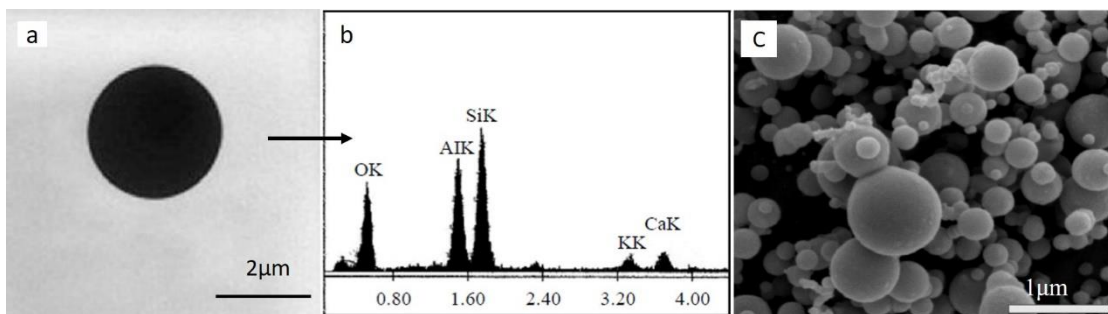


1557

1558 **Figure 5.** TEM images of metal particles. Elements of the detected parts of individual  
 1559 particles are in parentheses. (a) Zn-rich coatings with a rectangular Pb-rich inclusion,  
 1560 (b) Zn-rich coatings with quadrangular Pb-rich inclusions. (c) Aggregates of spherical  
 1561 Fe-rich particles. The images are from PM<sub>2.5</sub> samples collected in the haze episodes  
 1562 over northern China, 2007 (Li and Shao, 2009a).

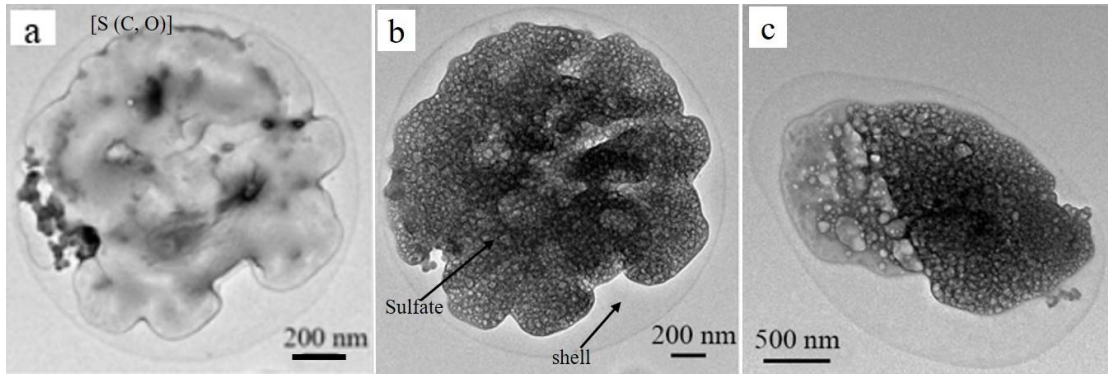
1563

1564



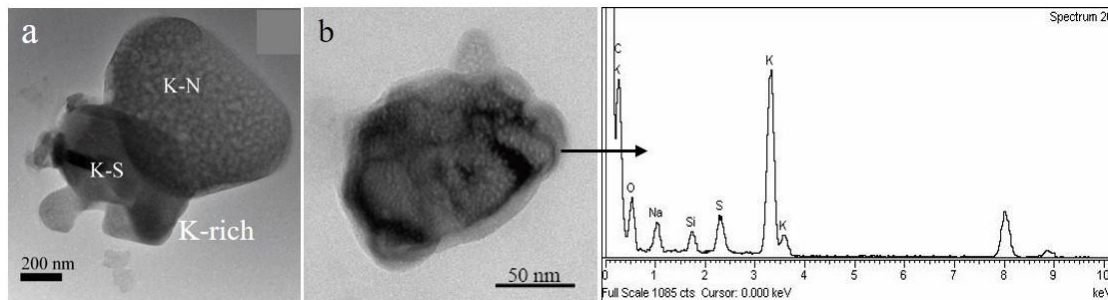
1565

1566 **Figure 6.** Electron microscopy images of fly ash particles. a The TEM image of a fly  
 1567 ash particle was from PM<sub>2.5</sub> collected in Beijing in spring 2011. b EDX spectrum of  
 1568 individual fly ash particle shown in a, c The SEM image of fly ash particles from PM<sub>10</sub>  
 1569 collected at the coking plants in Beijing. a and b are from Li et al. (2013b) and c is from  
 1570 Shao et al. (2016b).



1571  
 1572 **Figure 7.** TEM images of sulfate particles. a Sulfate particle in foam-like' structure  
 1573 shape, b and c Sulfate particles with core-shell structure shapes. The images were from  
 1574 PM<sub>2.5</sub> collected in a tunnel environment in Shenzhen 2014 (Hou, 2017).

1575  
 1576  
 1577  
 1578

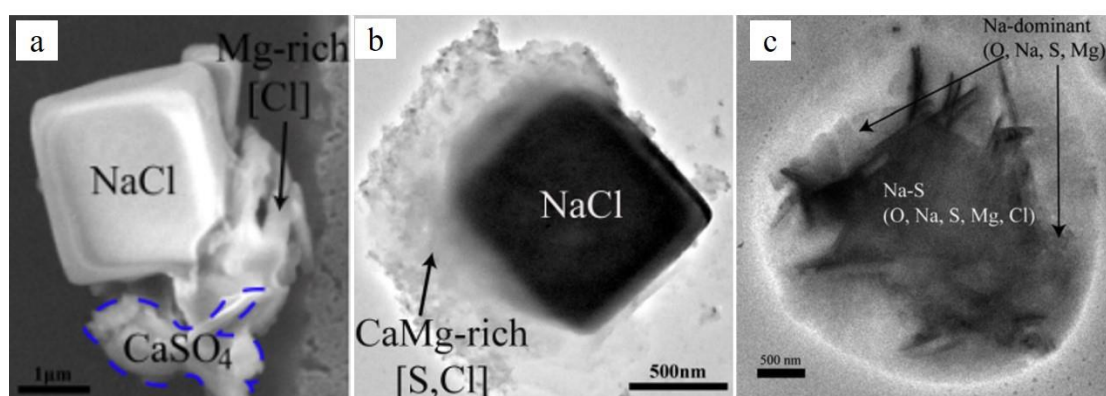


1579  
 1580 **Figure 8.** TEM image and EDX spectrum of K-rich particles. Image a was from PM<sub>2.5</sub>  
 1581 collected in the haze episodes over northern China, 2007 (Li and Shao, 2009a). Image  
 1582 b is from PM<sub>2.5</sub> collected from a bench experiment of biomass burning (Li, 2021).

1583



1584



1585

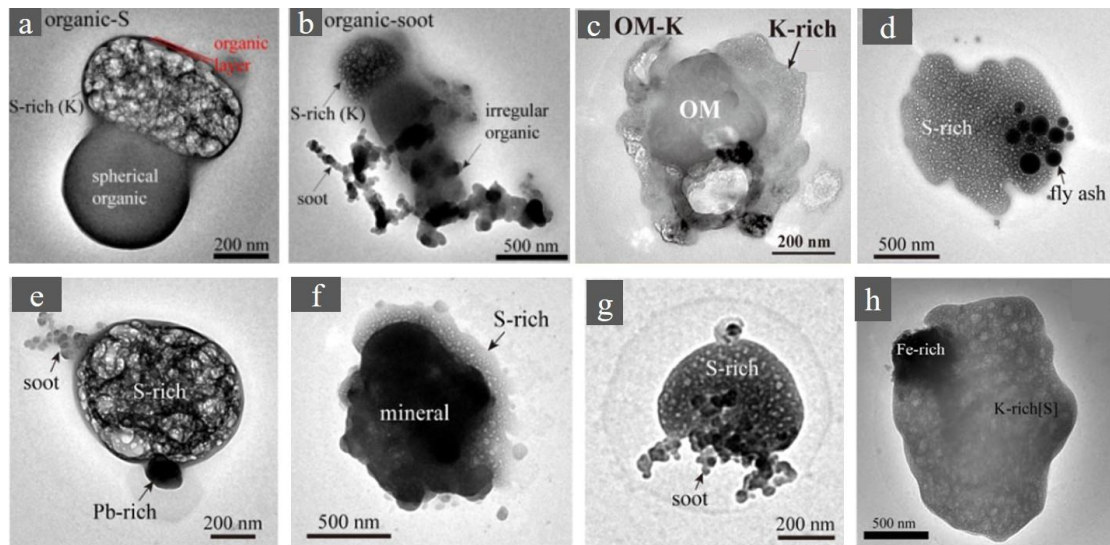
1586 **Figure 9.** Electron microscopy images of sea salt particles. a A fresh NaCl particle  
1587 observed in SEM, from aerosol sample collected in Svalbard in summer 2012. b A fresh  
1588 NaCl particle observed in TEM, from aerosol sample collected in Svalbard in summer  
1589 2012, c Amorphous NaCl particles were from aerosol sample collected in a south China  
1590 coastal city. a and b are from Chi et al. (2015) and c is from Li et al. (2010a, reproduced  
1591 with permission).

1592

1593

1594

1595



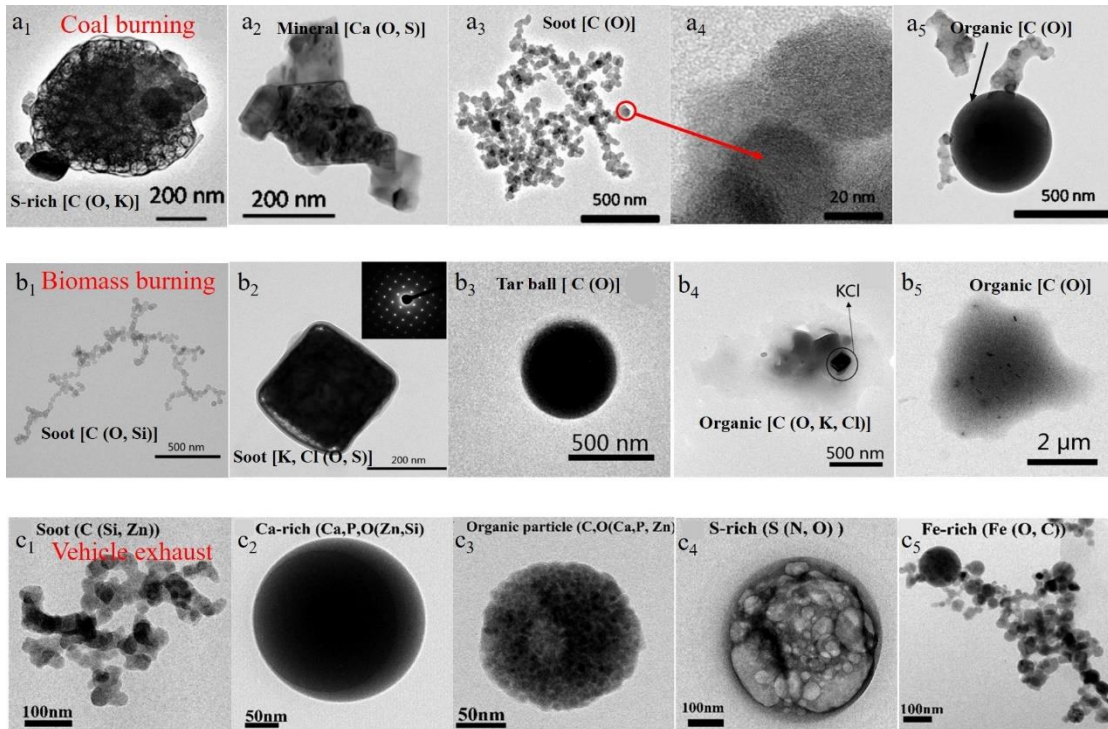
1597

1598 **Figure 10.** TEM images of some mixed particles. an organic and S-rich mixed particle  
 1599 was from PM<sub>2.5</sub> collected in haze episodes in in Northeast China (Zhang et al., 2017,  
 1600 reproduced with permission), b organic and soot mixed particle was from PM<sub>2.5</sub>  
 1601 collected in haze episodes in in Northeast China (Zhang et al., 2017, reproduced with  
 1602 permission), c organic and K-rich mixed particle was from aerosol sample collected in  
 1603 crop residue, wood, and solid waste combustion in a residential stove (Liu et al., 2017),  
 1604 d S-rich and fly ash mixed particle, e S-rich and metal mixed particle, f S-rich and  
 1605 mineral mixed particle, g S-rich and soot mixed particle, d-g were from PM<sub>2.5</sub>  
 1606 collected at a mountain site in North China 2014 (Liu et al., 2018), (h) K-rich and metal  
 1607 mixed particle were from aerosol sample collected in dust episodes over northern China  
 1608 2007 (Li and Shao, 2009b). All are mixed particles of irregular shape, except for g  
 1609 which is the mixed particle of core-shell structure.

1610

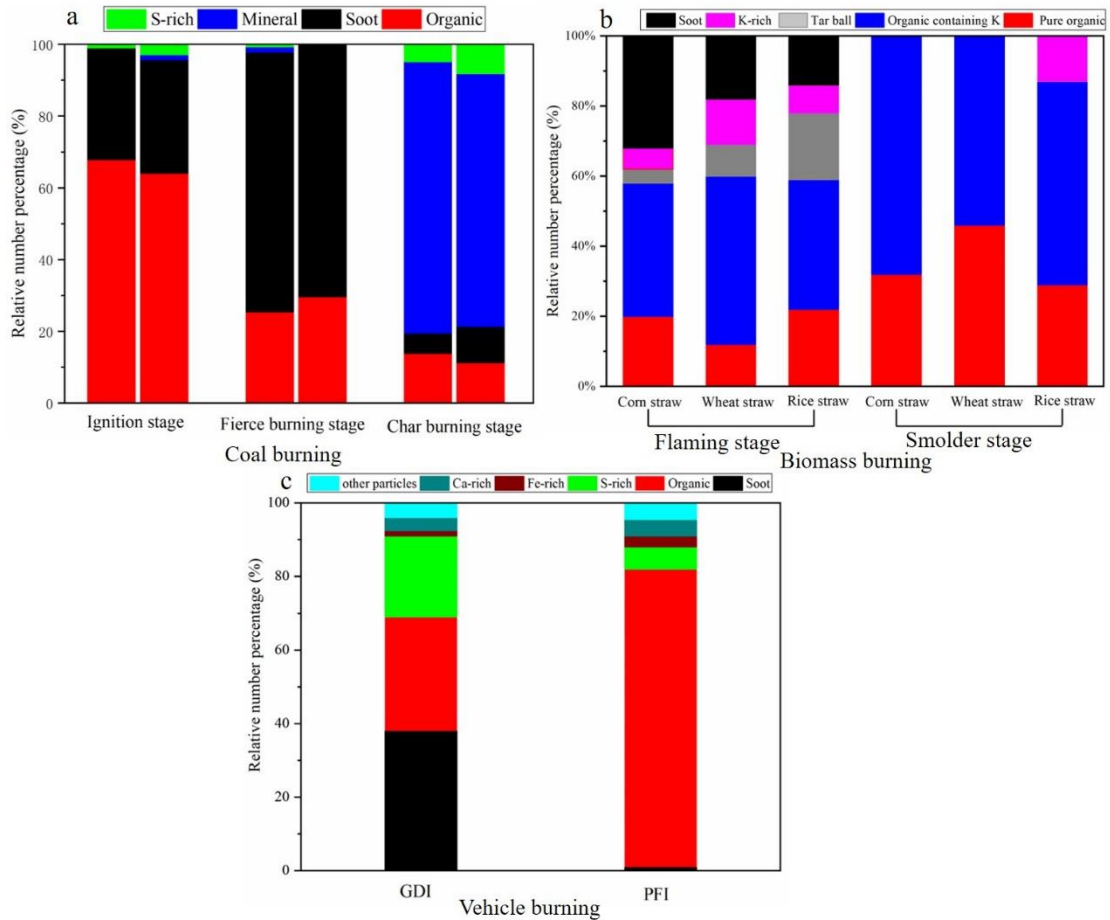


1611



1612

1613 **Figure 11.** Electron microscopy images of individual particles from the bench  
1614 experiments of coal burning, biomass burning and vehicle exhaust. a<sub>1</sub>-a<sub>5</sub> represent the  
1615 particles emitted by coal burning, b<sub>1</sub>-b<sub>5</sub> represent particles emitted by biomass burning,  
1616 c<sub>1</sub>-c<sub>4</sub> represent particles emitted by vehicle exhaust. a<sub>1</sub>, c<sub>4</sub> S-rich particle, a<sub>2</sub> mineral  
1617 particle, a<sub>3</sub>, b<sub>1</sub>, c<sub>1</sub> soot particle, a<sub>4</sub> Onion like structure of soot particle at high resolution,  
1618 a<sub>5</sub>, b<sub>5</sub>, c<sub>3</sub> organic particle; b<sub>2</sub> K-rich particle, b<sub>3</sub> tar ball, b<sub>4</sub> organic containing k particle,  
1619 c<sub>2</sub> Ca-rich particle, c<sub>5</sub> Fe-rich particle. The images of a<sub>1</sub> to a<sub>5</sub> are from Wang et al.  
1620 (2019a). The images of b<sub>1</sub> to b<sub>5</sub> are from Li (2021). The images of c<sub>1</sub> to c<sub>5</sub> are from  
1621 Xing (2018).



1622

1623 **Figure 12.** The relative percentage contents of different individual particle types were

1624 tested on the bench experiments of coal burning (a), biomass burning (b) and vehicle

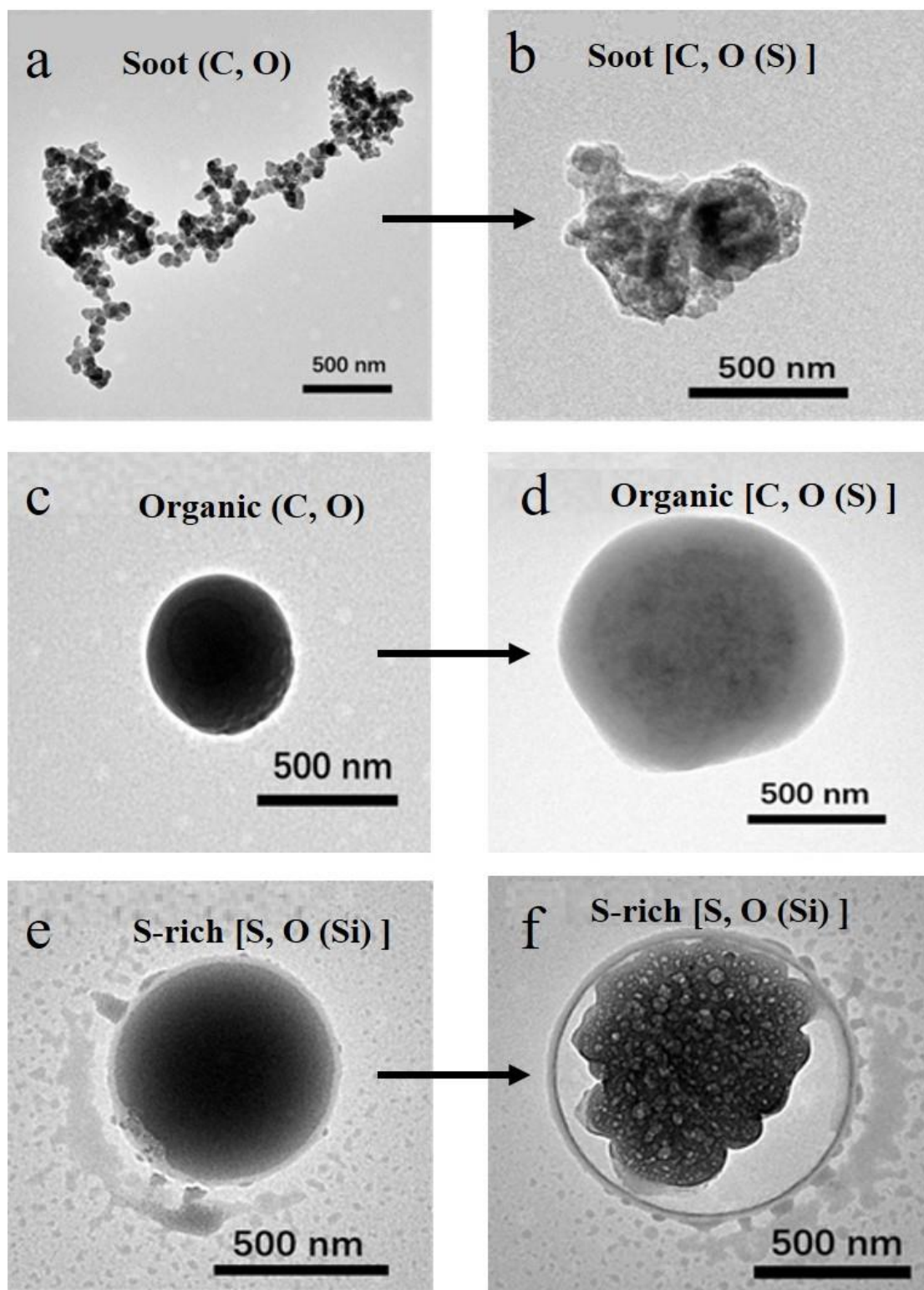
1625 exhaust (c). a, Coal-burning included the stages of ignition, fierce burning and char

1626 burning. b, Three types of straw in the flaming and smoldering stage. c, Vehicle exhaust

1627 included emissions from two engine types of GDI (gasoline-direct-injection) and PFI

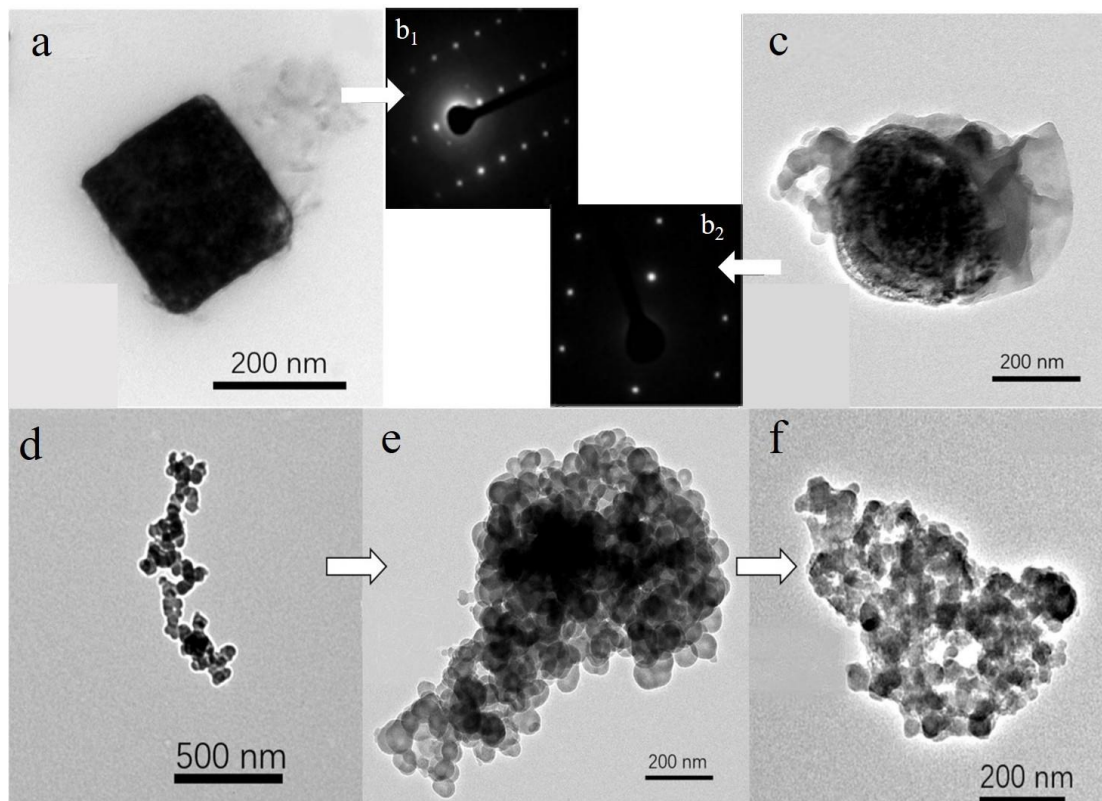
1628 (port fuel injection). The data for image a are from Wang et al. (2019a). The data for

1629 image b are from Li (2021). The data for image c are from Xing (2018).



1630

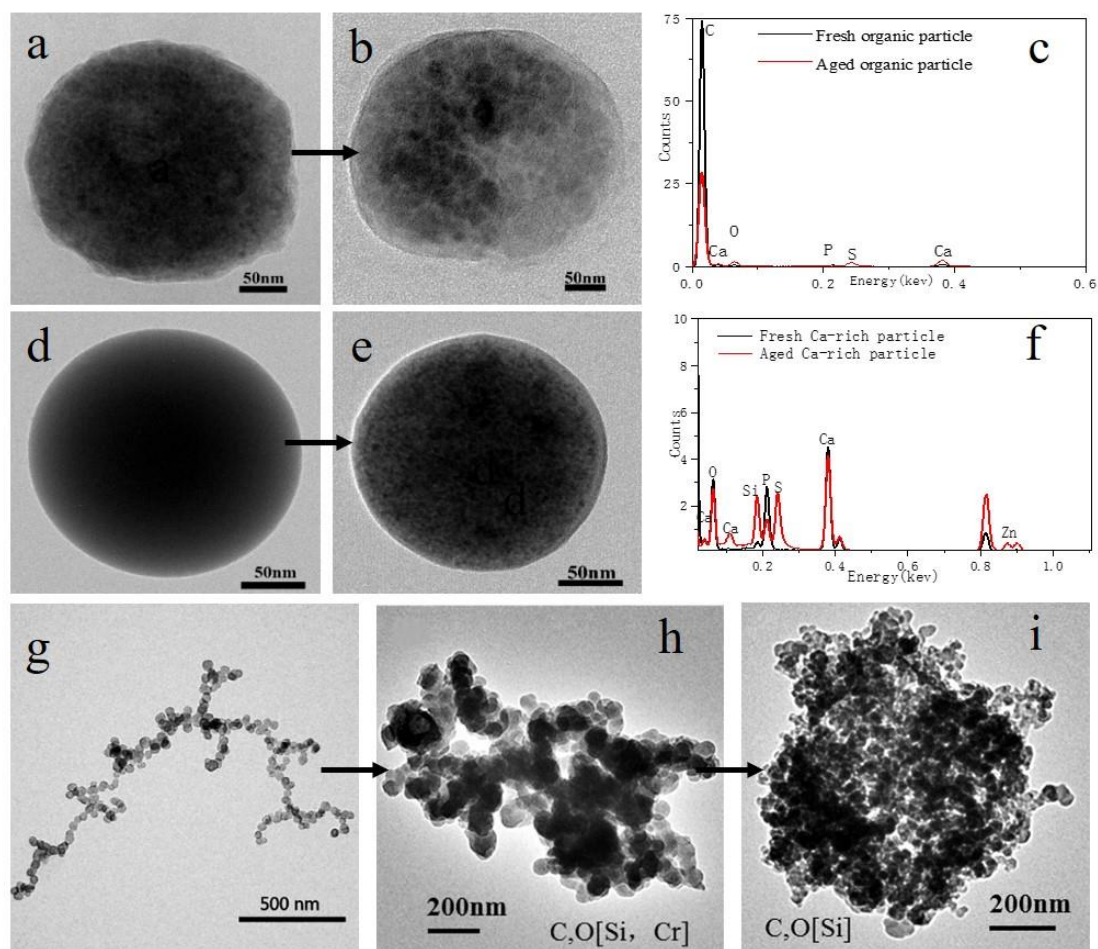
1631 **Figure 13.** Electron microscopy (TEM) images of individual particles (fresh and aged)  
 1632 from coal burning in smog chamber experiment. a Fresh soot particle; b Aged soot  
 1633 particles; c Fresh organic particle; d Aged organic particle; e Fresh sulfate particle; f  
 1634 Aged sulfate particle. The images are from Li (2021).



1635

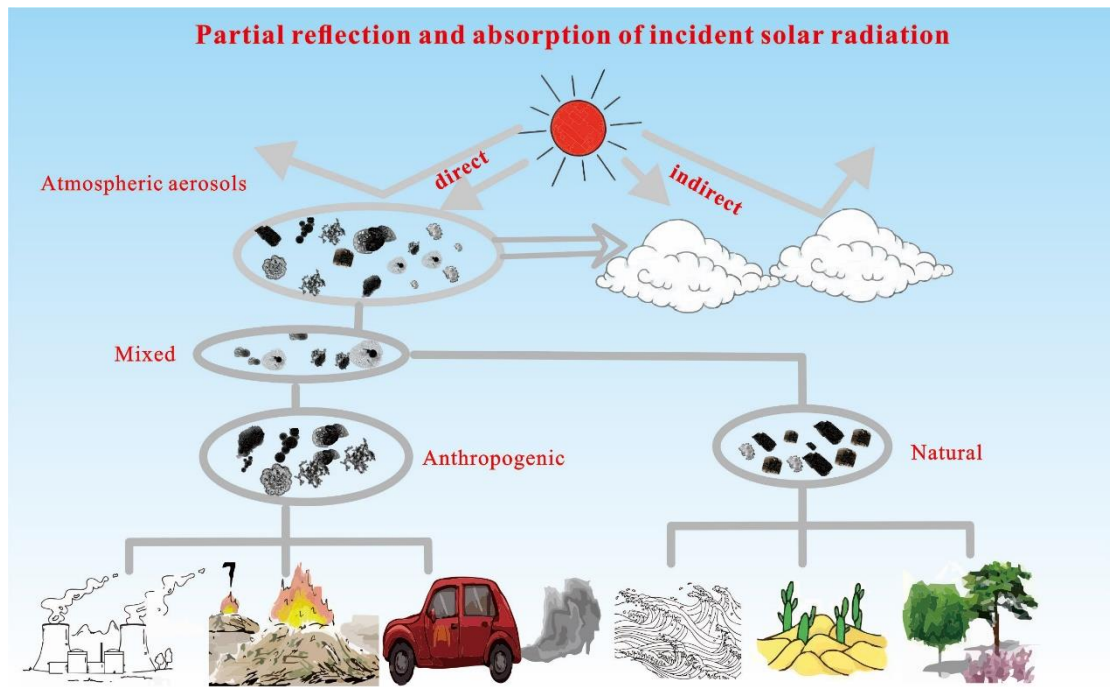
1636 **Figure 14.** Electron microscopy (TEM) images of individual particles (fresh and aged)  
 1637 from biomass burning in a smog chamber experiment. a KCl particles, b<sub>1</sub> Selected area  
 1638 electron diffraction of a, b<sub>2</sub> Selected area electron diffraction of c, c Amorphous KCl  
 1639 particles, d, e and f soot particles. The images are from Li (2021).





1640

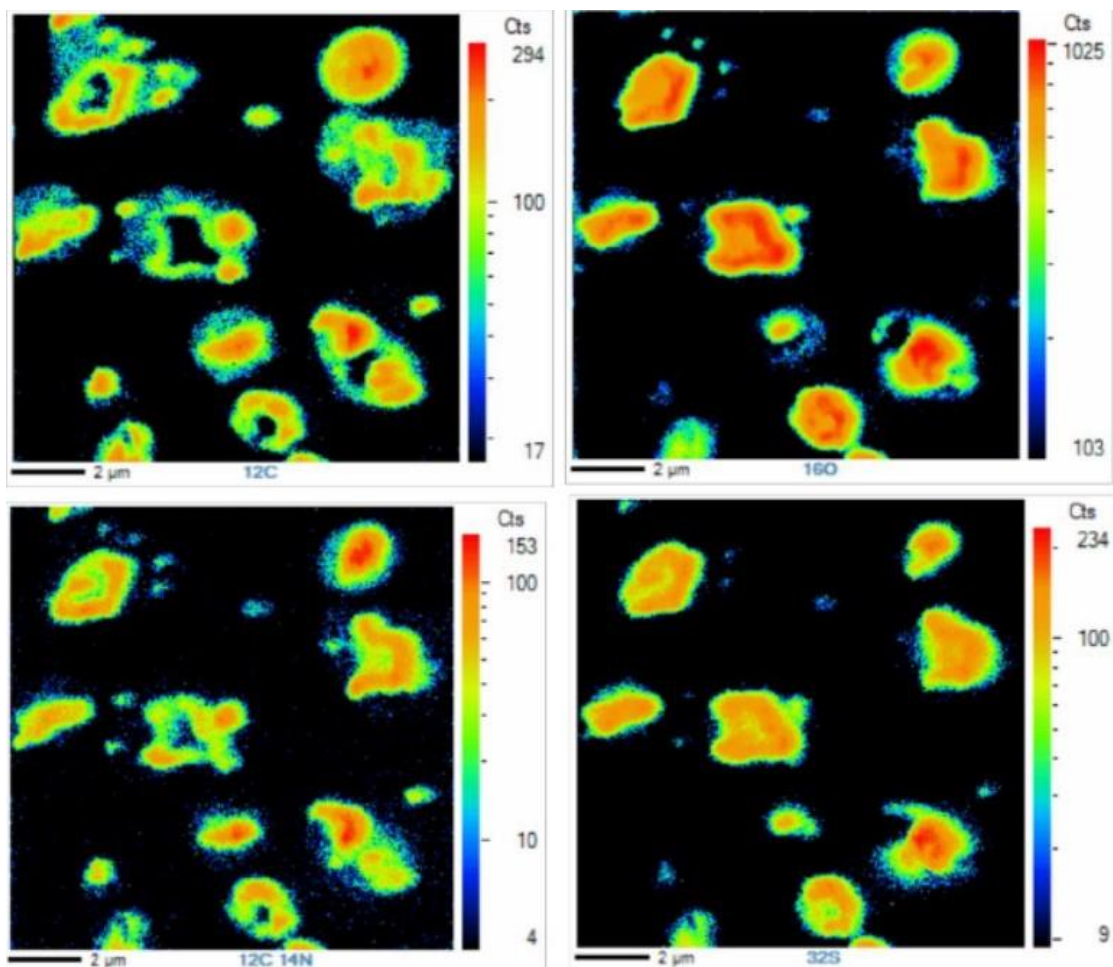
1641 **Figure 15.** Electron microscopy (TEM) images of individual particles (fresh and aged)  
 1642 from vehicle exhaust in a smog chamber experiment. a Fresh organic particle, b Aged  
 1643 organic particle, c EDX spectra of fresh and aged organic particles, d Fresh Ca-rich  
 1644 particle, e Aged Ca-rich particle, f EDX spectra of fresh and aged particles. g, h, i Soot  
 1645 particles. The images a-h are from Xing et al. (2020) and i is from Xing (2018).



1646

1647 **Figure 16.** Optical reflection and absorption of aerosols and cloud under incoming solar  
 1648 radiation. Atmospheric particles emitted from natural and anthropogenic sources can  
 1649 mix with each other, and mixed and unmixed particles can directly absorb and reflect  
 1650 solar radiation. Some particles can form CCN that absorb and reflect solar radiation,  
 1651 causing the indirect climate effects.

1652

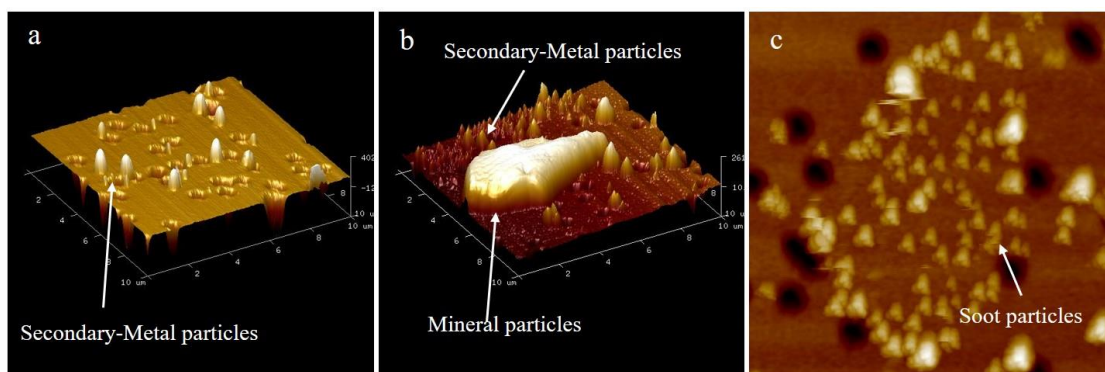


1653

1654 **Figure 17.** NanoSIMS images of organic and sulfate mixed particles.  $C^{14}N^-$  represents  
 1655 the distribution of organic matter content, and  $^{32}S^-$  and  $^{16}O^-$  represent the distribution  
 1656 of sulfate content in particles. The images were from  $PM_{2.5}$  collected at the road in  
 1657 urban Beijing in winter (Xing, 2018).

1658

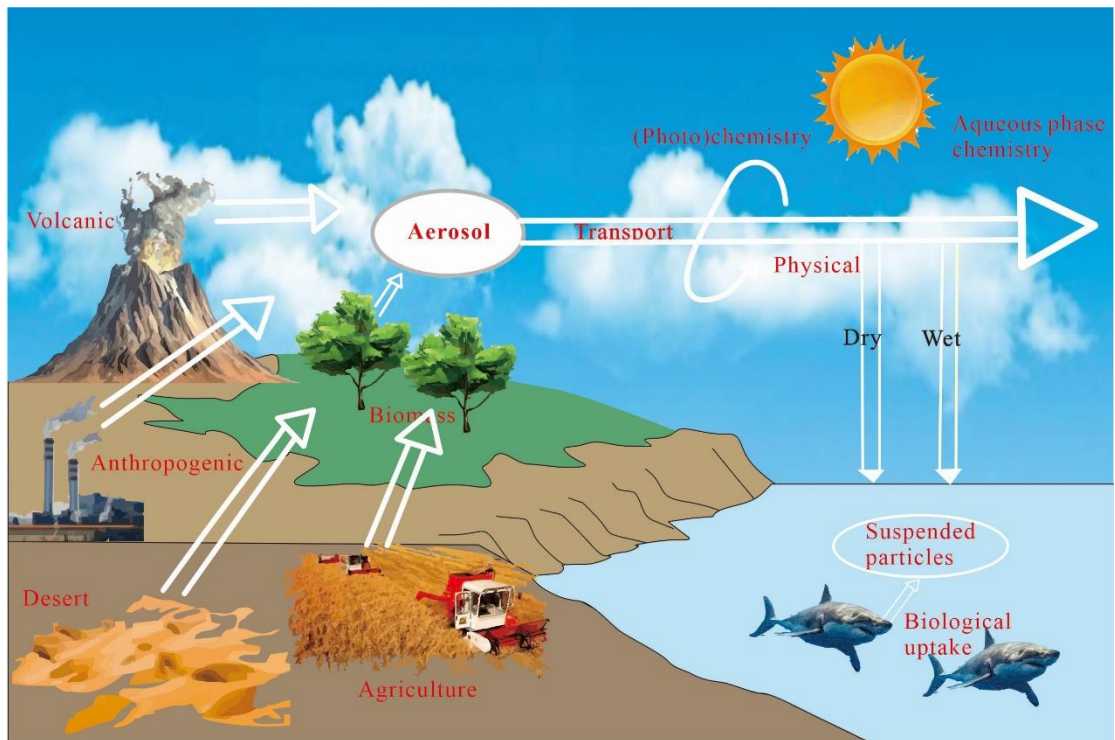
1659



1660

1661 **Figure 18.** AFM images of particles in PM<sub>2.5</sub>. a Metal and secondary mixed particles,  
1662 b Mineral particles and secondary mixed particles, c Soot particles. The images were  
1663 from PM<sub>2.5</sub> collected in a tunnel environment in Shenzhen 2014 (Hou, 2017). Aerosol  
1664 species are classified by TEM-EDX analysis.

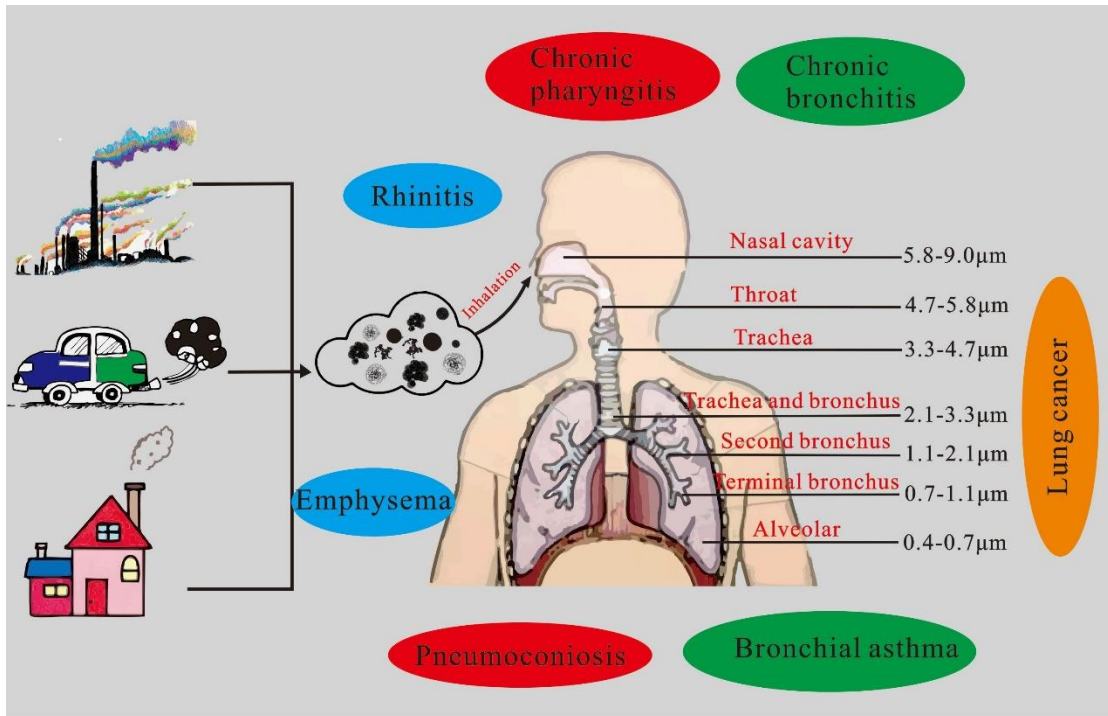
1665  
1666  
1667  
1668



1669  
1670 **Figure 19.** Schematic of aerosols impacts on the ocean. Atmospheric particles emitted  
1671 by natural and anthropogenic sources can be transported over great distances, affecting  
1672 local climate and biologicals.

1673





1674

1675 **Figure 20.** Health risks from exposure to particles in the atmosphere. Airborne particles  
 1676 with different sizes can reach different tissues (Nasal cavity, throat, trachea and  
 1677 bronchus, second bronchus, terminal bronchus and alveolar) in the body and cause  
 1678 corresponding diseases (Rhinitis, chronic pharyngitis, chronic bronchitis, bronchial  
 1679 asthma, pneumoconiosis, emphysema and lung cancer).

1680

1681

1682 **Table Captions**

1683 Table 1 Summary of analytical methods for individual particles

Methods	Size	Morphology	Advantages and drawbacks
Scanning Electron Microscopy (SEM)	best for >100 nm particle	3D particle shape	Low spatial and compositional specificity; only surface information in images
Transmission Electron Microscopy (TEM)	best for <2nm particle	2D particle shape	High spatial specificity for shape, manually operated and labor-intensive, resulting in poor statistics
Surface-Enhanced Raman Scattering (SERS)	best for <10nm particles	No information	The evaporation information of sulfate under vacuum conditions can be observed but no images
Scanning Transmission X-ray Microscopy (STXM-NEXAFS)	best for >100 nm particle	2D particle shape	Specific bond types can be studied in carbonaceous aerosol; synchrotron radiation needed. low spatial resolution
Atomic Force Microscope (AFM)	best for <2nm particle	3D particle shape	The surface texture, viscosity, deformation, and elasticity of the particle can be studied, but the composition of the particle cannot be provided
Nanometer - scale Secondary Ion Mass Spectrometer (Nano - SIMS)	best for >50 nm particle	2D particle shape	Specific bond types can be studied, manually operated and labor-intensive, resulting in poor statistics
Time of Flight Secondary Ion Mass Spectrometer (TOF - SIMS)	best for >100 nm particle	2D particle shape	Specific bond types can be studied; low spatial resolution
Individual Aerosol Mass Spectrometer (SPAMS)	best for >100 nm particles	No information	The chemical composition and particle size of particulate matter can be obtained but no images

Aerosol-Time-Of-Flight Mass Spectrometer (ATOFMS)/Ultrafine aerosol time-of-flight mass spectrometer (UF-ATOFMS)	ATOOFMS, best for >100nm particles UF-ATOFMS, >50nm	No information	Specific bond types can be studied for inorganic and organic particle; online instrument for good statistics but no images
Micro-Raman Spectroscopy (Micro-RS)	best for >1µm particles	2D particle shape	Direct identification of molecules and functional groups in individual particles; Raman scattering intensity is easily affected by optical system parameters and other factors

1684  
1685

Table 2 The types of individual particles in PM2.5 based on TEM-EDX

Categories	Individual particle types		Major element	Morphologies	Major sources
Carbonaceous particles	Soot aggregates		C, O, and minor Si, K	Chain-like, cluster-like, and compact-like morphologies	Emissions from vehicles burning fossil fuel
	Organic particles	Primary organic particles	C and O	Spherical and near-spherical morphologies	Fossil fuel and biomass burning
		Secondary organic particles	C, O, and S	Irregular morphologies	Secondary conversion of volatile organic compounds (VOCs)
	Biological particles		C, O, P, K and Si	Irregular morphologies	Pollen and robes
Non-carbonaceous particles	Mineral particles		Si, Al, Ca, Mg, K, and Fe	Irregular morphologies	Road, construction, and crustal dust
	Metal particles		Zn, Fe, Pb, Mn, and minor Cr	Spherical and irregular morphologies	Coal-fired power plant, heavy industries, and tyre abrasion
	Fly ashes		Si, Al, Fe and minor Na, K	Spherical morphology	Coal combustion
	S-rich particles		S and minor Na, K, Ca	Irregular morphologies and core-shell structure	Derived from SO <sub>2</sub> emitted from coal combustion or vehicles
	K-particles		K, N, S and Cl	Irregular morphologies	Biomass burning
	Sea salt particles		Na, Cl and S	Cubic crystalline morphology	Ocean and blowing snow
Mixed particles	Mixture of above particles		Complicated composition	Irregular morphologies and core-shell structure	Heterogeneous reaction of particles

1689 Table 3 Common types of the internal mixed particles in terms of compositions

---

organic and sulfate mixed particles

organic and soot mixed particles

organic and K-rich mixed particles

S-rich and fly ash mixed particles

S-rich and metal mixed particles

S-rich and mineral mixed particles

S-rich and soot mixed particles

K-rich and metal mixed particles

---

1690

1691

Abbreviation	
ACMS	Aerosol Chemical Speciation Monitoring
AFM	Atomic Force Microscopy
AMS	Aerosol Mass Spectrometry
APPCAP	Air Pollution Prevention and Control Action Plan
ATOFMS	Aerosol-Time-Of-Flight Mass Spectrometry
CCN	Cloud Condensation Nuclei
EDX	Energy Dispersive X-ray Spectroscopy
EPMA	Electron Probe X-ray Micro-Analysis
GDI	Gasoline-Direct-Injection
HPLC/MS	High Performance Liquid Chromatography Mass Spectrometry
IC	Ion Chromatograph
ICP-AES	Inductively Coupled Plasma Atomic Emission Spectrometry
ICP-MS	Inductively Coupled Plasma Mass Spectrometer
ICP-OES	Inductively Coupled Plasma-Optical Emission Spectroscopy
GC-MS	Gas Chromatograph Mass Spectrometry
K-rich	Potassium-rich
Micro-PIXE	Micro-Particle-Induced X-ray Emission
Nano-SIMS	Nanometer-Scale Secondary Ion Mass Spectrometer
NMVOCs	Non-Methane Volatile Organic Compounds
OM	Organic Matter
PFI	Port Fuel Injection
POM	Primary Organic Matter
PTR-MS	Proton Transfer Reaction Mass Spectrometry
SEM	Scanning Electron Microscopy
SERS	Surface-Enhanced Raman Scattering
SOA	Secondary Organic Aerosols
SOM	Secondary Organic Matter
SPAMS	Single Particle Aerosol Mass Spectrometry
STXM	Scanning Transmission X-ray Microscopy
TEM	Transmission Electron Microscopy
TOF-SIMS	Time Of Flight Secondary Ion Mass Spectrometry
VOCs	Volatile Organic Compounds